TURBINE BLADE PLATFORM FILM COOLING WITH SIMULATED STATOR-ROTOR PURGE FLOW WITH VARIED SEAL WIDTH AND UPSTREAM WAKE WITH VORTEX

A Thesis

by

SARAH ANNE BLAKE

Submitted to the Office of Graduate Studies of
Texas A&M University
in partial fulfillment of the requirements for the degree of

MASTER OF SCIENCE

May 2007

Major Subject: Mechanical Engineering

TURBINE BLADE PLATFORM FILM COOLING WITH SIMULATED STATOR-ROTOR PURGE FLOW WITH VARIED SEAL WIDTH AND UPSTREAM WAKE WITH VORTEX

A Thesis

by

SARAH ANNE BLAKE

Submitted to the Office of Graduate Studies of
Texas A&M University
in partial fulfillment of the requirements for the degree of

MASTER OF SCIENCE

Approved by:

Chair of Committee,	Je-Chin Han
Committee Members,	Sai Lau
	Hamn-Ching Chen
Head of Department,	Dennis L. O'Neal

May 2007

Major Subject: Mechanical Engineering

ABSTRACT

Turbine Blade Platform Film Cooling with Simulated Stator-Rotor Purge Flow with Varied Seal Width and Upstream Wake with Vortex. (May 2007)
Sarah Anne Blake, B.S., University of Maine
Chair of Advisory Committee: Dr. Je-Chin Han

The turbine blade platform can be protected from hot mainstream gases by injecting cooler air through the gap between stator and rotor. The effectiveness of this film cooling method depends on the geometry of the slot, the quantity of injected air, and the secondary flows near the platform. The purpose of this study was to measure the effect of the upstream vane or stator on this type of platform cooling, as well as the effect of changes in the width of the gap.

Film cooling effectiveness distributions were obtained on a turbine blade platform within a linear cascade with upstream slot injection. The width of the slot was varied as well as the mass flow rate of the injected coolant. Obstacles were placed upstream to model the effect of the upstream vane. The coolant was injected through an advanced labyrinth seal to simulate purge flow through a stator-rotor seal. The width of the opening of this seal was varied to simulate the effect of misalignment. Stationary rods were placed upstream of the cascade in four phase locations to model the unsteady wake formed at the trailing edge of the upstream vane. Delta wings were also placed in four positions to create a vortex similar to the passage vortex at the exit of the vane. The film cooling effectiveness distributions were measured using pressure-sensitive paint (PSP). Reducing the width of the slot was found to decrease the area of coolant coverage, although the film cooling effectiveness close to the slot was slightly increased. The unsteady wake was found to have a trivial effect on platform cooling, while the passage vortex from the upstream vane may significantly reduce the film cooling effectiveness.

ACKNOWLEDGEMENTS

I would like to thank Dr. Je-Chin Han for the opportunity to pursue this research in his laboratory and for his guidance. I am grateful to Dr. Sai Lau and Dr. Hamn-Ching Chen for serving on my committee. I would also like to thank all my colleagues who have assisted me in the laboratory, especially Dr. Lesley Wright for teaching me the PSP measurement technique and so much more, Dr. Dong-Ho Rhee for providing CFD modeling and help taking data, and Joshua Grizzle for helping me to take data.

Finally, I would like to thank my husband for all his support. I also appreciate the support of my parents and sisters, who have always encouraged me to succeed.

NOMENCLATURE

C_{ax}	axial chord length of the blade
C_{mix}	oxygen concentration of mainstream-coolant mixture mix
C_{∞}	oxygen concentration of mainstream
I	emission intensity of PSP
I_{air}	emission intensity of PSP recorded with air as the coolant
I_{N2}	emission intensity of PSP recorded with nitrogen as the coolant
I_{ref}	emission intensity of PSP at reference (atmospheric) pressure
M_s	slot injection blowing ratio, ratio of coolant momentum to mainstream momentum
m_s	slot injection mass flow ratio (percentage of the mainstream flow)
$(P_{O2})_{N2}$	partial pressure of oxygen measured with nitrogen as the coolant
$(P_{O2})_{air}$	partial pressure of oxygen measured with air as the coolant
Tu	turbulence intensity
w	slot width (m)
x	axial distance from the cascade leading edge (m)
θ	delta wing orientation with respect to inlet mainstream flow
η	film cooling effectiveness

TABLE OF CONTENTS

Page

INTRODUCTION 1

Endwall and Platform Heat Transfer 1
Film Cooling of Endwall and Platform 2
Effect of Upstream Vane 4
Current Study 6

EXPERIMENTAL SETUP AND PROCEDURE 8

Low-Speed Wind Tunnel 8
Linear Cascade 9
Stator-Rotor Seal 9
Upstream Wake and Vortex Generation 10
Pressure-Sensitive Paint Measurement Technique 12
Instrumentation 15

RESULTS 17

Baseline Case 18
Stationary Rods 19
Delta Wings 20
Rods and Delta Wings 23
Varied Seal Width 25
Laterally Averaged Film Cooling Effectiveness 31
Expected Heat Transfer Coefficients 44

CONCLUSIONS 45

Recommendations 46

REFERENCES 47

APPENDIX A 52

APPENDIX B 61

VITA 66

LIST OF FIGURES

FIGURE Page

1 Rod and Delta Wing Conceptual Flows (a) Unsteady Wake, (b) Rod Generated Unsteady Wake, (c) Passage Vortex in Vane [6], (d) Vortex Generated by Delta Wing 6

2 Detail of Low Speed Wind Tunnel and Turbine Blade Cascade 8

3 Platform Film Cooling Configuration (a) Detail of Cooled Platform with Rod and Delta Wing, (b) Detail of Labyrinth-Like Stator-Rotor Seal, (c) Detail of Rod and Delta Wing 10

4 Rod and Delta Wing Positions In Reference to Stagnation Lines 11

5 Flow in Cooled Passage 12

6 Calibration Curve for Pressure Sensitive Paint Relating Intensity and Pressure Ratios 14

7 Experimental Setup and Instrumentation 16

8 Film Cooling Effectiveness on Platform with Freestream Turbulence of 5%, w = 4.4mm and Various Seal Injection Rates 18

9 Film Cooling Effectiveness on Platform with Wake Rod in Four Positions and m_s = 1.0% 20

10 Film Cooling Effectiveness on Platform with Delta Wing in Four Positions, m_s = 1.0% and θ = 30° 21

11 Film Cooling Effectiveness on Platform with Delta Wing in Four Positions, m_s = 1.0% and θ = 45° 22

12 Film Cooling Effectiveness on Platform with Wake Rod and Delta Wing in Four Positions, m_s = 1.0% and θ = 45° 24

FIGURE Page

13 Film Cooling Effectiveness on Platform with Wake Rod and Delta Wing in Position 4, $\theta = 45°$ and Various Seal Injection Rates 25

14 Film Cooling Effectiveness on Platform with Freestream Turbulence of 5%, w = 0.30 cm and Various Seal Injection Rates 27

15 Film Cooling Effectiveness on Platform with Freestream Turbulence of 5%, w = 0.15 cm and Various Seal Injection Rates 28

16 Film Cooling Effectiveness on Platform with Delta Wing in Four Positions, $m_s = 1.0\%$, $\theta = 45°$ and w = 0.30 cm 29

17 Film Cooling Effectiveness on Platform with Delta Wing in Four Positions, $m_s = 1.0\%$, $\theta = 45°$ and w = 0.15cm 30

18 Comparison of Laterally Averaged Film Cooling Effectiveness on the Platform for Various Upstream Conditions, $m_s = 0.5\%$ and w = 4.4 mm 32

19 Comparison of Laterally Averaged Film Cooling Effectiveness on the Platform for Various Upstream Conditions, $m_s = 1.0\%$ and w = 4.4 mm 33

20 Comparison of Laterally Averaged Film Cooling Effectiveness on the Platform for Various Upstream Conditions, $m_s = 1.5\%$ and w = 4.4 mm 34

21 Comparison of Laterally Averaged Film Cooling Effectiveness on the Platform for Various Upstream Conditions, $m_s = 2.0\%$ and w = 4.4 mm 35

22 Comparison of Laterally Averaged Film Cooling Effectiveness on the Platform for Various Slot Widths, $\theta = 45°$ and $m_s = 0.5\%$ 37

23 Comparison of Laterally Averaged Film Cooling Effectiveness on the Platform for Various Slot Widths, $\theta = 45°$ and $m_s = 1.0\%$ 38

24 Comparison of Laterally Averaged Film Cooling Effectiveness on the Platform for Various Slot Widths, $\theta = 45°$ and $m_s = 1.5\%$ 39

25 Comparison of Laterally Averaged Film Cooling Effectiveness on the Platform for Various Slot Widths, $\theta = 45°$ and $m_s = 2.0\%$ 40

FIGURE Page

26 Comparison of Pitchwise Film Cooling Effectiveness for Various Slot Widths and Blowing Rates, Without Delta Wing and With Delta Wing in Position 4 43

LIST OF TABLES

TABLE Page

1 Experimental Conditions 17

2 Blowing Rates and Blowing Ratios 26

INTRODUCTION

Gas turbine engines power aircraft and other vehicles and are used to produce electricity. In order to make these engines more powerful and more efficient, the temperature of the gases exiting the combustor has been increased beyond the safe working temperature for the blades and other parts. Internal and external cooling must be used to keep these parts at safe temperatures. External cooling or film cooling involves injecting cooler air from the compressor through holes in the surface of a part to create a layer of relatively cool air between the surface and the hot gas. A good film cooling design provides adequate protection over the entire surface while using as little coolant as possible, to minimize aerodynamic losses.

Endwall and Platform Heat Transfer

Film cooling has been utilized to protect the vane endwall and blade platform. Reviews published by Han et al. [1], Langston [2], Chyu [3], and Simon and Piggush [4] provide an overview of endwall and platform studies. These studies provide information about the flow near the platform and the heat transfer to the platform, as well as methods and effectiveness of film cooling. Complex secondary flows exist near the platform increasing heat transfer. Due to these complex flows, cooling the platform evenly is difficult.

Langston et al. [5, 6] presented complete flow measurements near the endwall of a turbine vane. They showed that as the inlet boundary layer approaches a vane, a horseshoe vortex forms near the intersection of the vane and endwall. One leg of the horseshoe vortex follows the suction side of the vane. The other leg continues onto the pressure side of the vane, but the pressure gradient across the passage causes the pressure-side leg to move across the passage toward the suction side of the adjacent

---

This thesis follows the style of ASME Journal of Turbomachinery.

vane. The pressure-side leg combines with the cross-flow in the passage and captures additional fluid from the mainstream, forming the passage vortex. Goldstein and Spores [7] used the naphthalene sublimation method to measure heat transfer coefficients on the endwall. Their results showed that the passage vortex and the suction-side leg of the horseshoe vortex lift off the endwall and continue along the suction side of the vane. They also confirmed the presence of smaller corner vortices where each vane surface meets the endwall. Wang et al. [8] used multiple smoke-wire visualization and also noted the presence of small, intense vortices at the junctions between the vane surfaces and the endwall.

Film Cooling of Endwall and Platform

Most early studies of film cooling on the endwall used coolant injected through discrete holes. Takeishi et al. [9] measured the heat transfer coefficients and film cooling effectiveness on the endwall and vane surfaces for a cooled, fully-annular, three-dimensional vane. They found that the secondary flows strongly influenced heat transfer on the suction side of the vane and on the endwall but had little effect on the pressure side of the vane. Harasgama and Burton [10] found that four rows of film cooling holes placed on iso-Mach lines could cool an endwall quite effectively, but the pressure side of the passage remained uncooled. Jabbari et al. [11] used 14 discrete film cooling holes and found that the film cooling effectiveness varied greatly for the 60 points that they measured. They confirmed with ammonium-diazo traces that the coolant was swept toward the suction side.

Friedrichs et al. [12, 13] developed a technique for quantitatively measuring the film cooling effectiveness using ammonia and diazo. They measured the film cooling effectiveness for a simple endwall cooling design using four rows of holes and confirmed that the spread of coolant depended heavily on the secondary flows in the passage and not on the direction of the holes. They found several areas that were not cooled by their simple design. A later study by Friedrichs et al. [14] used a new cooling

design based on the results of their previous studies. They placed the coolant holes in regions of high static pressure and provided much more even coverage for the endwall, though some portions near the leading edge and the suction side of the blade remained uncooled.

A recent study by Barigozzi [15] studied the effect of fan-shaped holes as opposed to cylindrical holes for endwall film cooling. They measured the secondary flows using a miniature 5-hole probe, as well as the film cooling effectiveness using thermochromic liquid crystals. They found that fan-shaped holes provide better protection than cylindrical holes, especially for higher coolant mass flow rates, and the increases in aerodynamic losses were small.

On the blade surfaces, film cooling through slots is generally impractical due to structural considerations. On the endwall, slot cooling is common. In fact, relatively cool air is typically injected through the gap between the combustor and vane or the vane and the rotor, in order to prevent hot gases from entering. This cool air can be utilized for film cooling of the endwall. In an early study of slot cooling on the endwall, Blair [16] found that the coolant was swept toward the suction side, leaving the pressure side unprotected.

Granser and Schulenberg [17] showed that coolant from an upstream slot can reduce the secondary flows in the passage by increasing the momentum of the boundary layer. Similarly, coolant slots used by Roy et al. [18] reduced the heat transfer near the leading edge. Burd et al. [19] and Oke et al. [20, 21] also studied film cooling through slots upstream of vanes. They found coolant from the slot could provide coverage for most of the passage. Nicklas [22] measured the film cooling effectiveness and heat transfer coefficients for a vane endwall with upstream slot injection and discrete holes. They found that due to the location of their slot the horseshoe vortex was strengthened, increasing the heat transfer coefficients near the leading edge. However, the discrete

holes decreased the effect of the passage vortex on the endwall, reducing the heat transfer coefficients in that region. Liu et al. [23] confirmed that film cooling effectiveness for upstream injection is strongly influenced by secondary flows and can be improved by increasing the blowing ratio.

Zhang and Jaiswal [24] measured the film cooling effectiveness of a single row of upstream slots or a double row of holes on a vane endwall. They found that higher coolant mass flow rates decreased the passage secondary flows, drastically increasing the film cooling effectiveness. The slots provided more even coverage across the passage, but the double row of holes provided higher film cooling effectiveness near the trailing edge. Zhang and Moon [25] investigated the effect of a backward-facing step. Knost and Thole [26] used upstream slot injection in combination with two different cooling hole configurations. They were able to provide cooling for difficult areas, but the center of the passage was overcooled. They showed that slot cooling and discrete hole film cooling influence one another when used together. Cardwell et al. [27] found that misalignment between adjacent vanes can reduce the effectiveness of upstream slot injection. For high blowing ratios, they found that a rough endwall surface decreased the film cooling effectiveness, but the effect was much less for low blowing ratios.

Studies by Wright et al. [28 - 30] examined the film cooling effectiveness on a turbine rotor platform for various stator-rotor seal geometries. They found that for low coolant flow rates secondary flows prevent coolant from reaching a large portion of the passage on the pressure side. For higher coolant flow rates, the effect of the secondary flows was reduced and coverage was provided for most of the platform.

Effect of Upstream Vane

Numerous studies have found that the secondary flows in a vane or rotor passage greatly affect film cooling. However, most of the studies have been performed on linear cascades or turbine vanes, so the effect of the upstream vane on rotor platform cooling

has not been examined. Han et al. [31] found that the unsteady wake from the trailing edge of the vane affects the heat transfer coefficients on the rotor blade midspan. They used rotating rods placed upstream of the blades to simulate the relative motion of the blades with respect to the vanes. As shown in Figure 1, a wake forms downstream of the vane, and this wake will influence flow around the turbine blades. Cylindrical rods can be used to model this interaction, and create a wake similar to that created by the trailing edge of the vane. The unsteady wake caused boundary layer transition to occur closer to the leading edge, leading to significantly higher heat transfer coefficients. The effect varied with both Reynolds number and Strouhal number. Ou et al. [32] found this effect to be secondary to the increase in heat transfer coefficients caused by film cooling. Zhang and Han [33, 34] extended this study to include the effect of mainstream turbulence. Both increased mainstream turbulence and unsteady wake individually increase the heat transfer coefficients on the midspan of the blade, but with high mainstream turbulence the effect of the unsteady wake is reduced. Similarly, with the unsteady wake present, increasing the mainstream turbulence has a reduced effect. Mhetras and Han [35] used stationary rods to simulate the unsteady wake effect by measuring the film cooling effectiveness on the blade surface with the rods in each of four positions; this method showed the instantaneous wake effect rather than the average effect of the wake. Due to the wake created by the rods, the film cooling effectiveness was reduced, especially on the suction side of the blade.

On the rotor platform, it is possible that secondary flows from the vane endwall also affect heat transfer and film cooling. Nicklas [22] found that downstream of the vane the passage vortex was the main influence on heat transfer, so it is likely that this effect would continue onto the rotor platform. Several groups [36 – 40] are trying to reduce the passage vortex by modifying the blade-endwall junction, but it is still important to know how the passage vortex may influence rotor platform cooling.

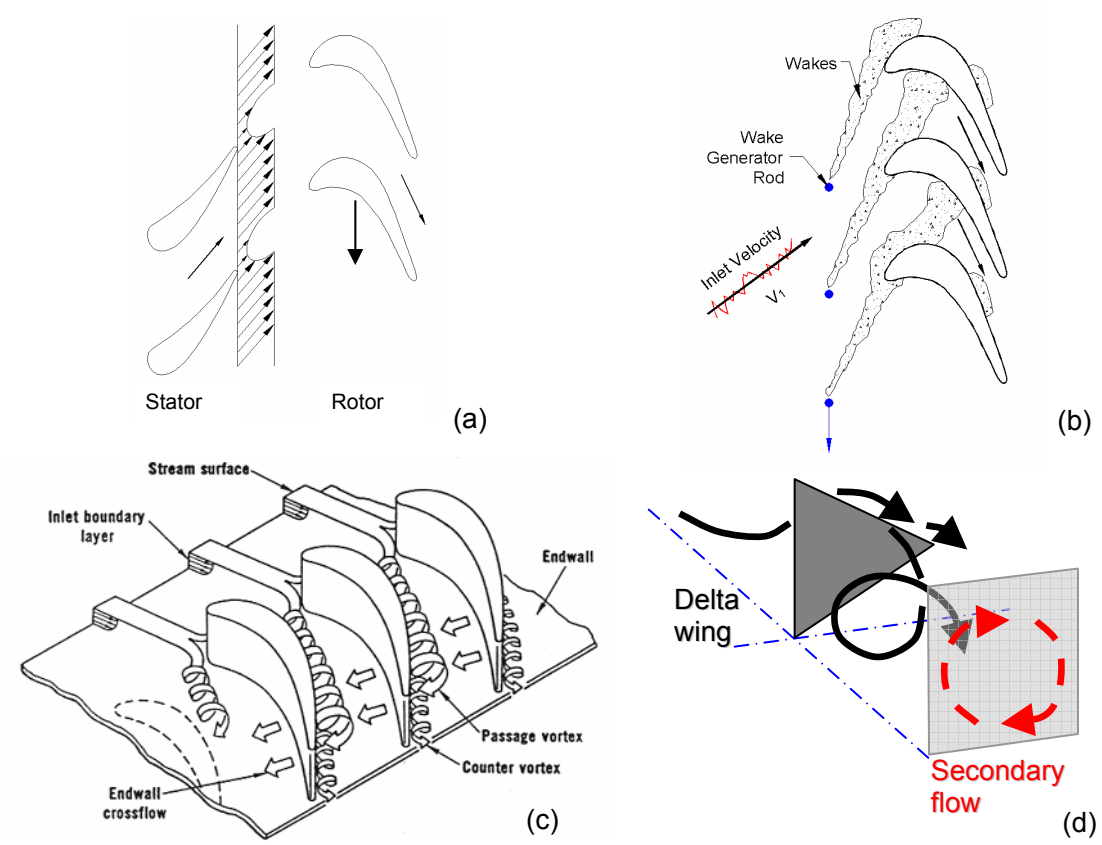

Figure 1: Rod and Delta Wing Conceptual Flows (a) Unsteady Wake, (b) Rod Generated Unsteady Wake, (c) Passage Vortex in Vane [6], (d) Vortex Generated by Delta Wing

Current Study

The objective of the current study is to determine how misalignment between the stator and rotor may affect how well purge flow from the stator-rotor seal protects the blade platform. Also, the effect of the upstream vane on turbine rotor cooling will be evaluated. The width of the coolant slot will be varied to simulate misalignment. Stationary rods and delta wings will be placed upstream of the blades to simulate the wake created at the trailing edge of the vane and the passage vortex created in the vane. The rods will be placed at four different spanwise positions to determine the effect of the unsteady wake at various points in time as the rotor passes by the vane. The delta wings

will placed in four similar positions and at two different angles to the mainstream flow, to vary the vortex strength. Finally, the combined effect of the rods and delta wings will be tested. For each upstream condition and slot width tested, the coolant flow rate will be varied between 0.5 and 2.0% of the mainstream flow rate.

EXPERIMENTAL SETUP AND PROCEDURE

Low-Speed Wind Tunnel

The film cooling effectiveness was measured on the platform within a linear cascade of high pressure turbine blades, in an open-loop wind tunnel, as shown in Figure 2. A 4.5:1 contraction nozzle with two mesh screens guides the flow into the test area, which is 25.4 cm high and 75.0 cm wide. The wind tunnel operates in suction. The velocity is controlled by a variable frequency controller attached to a 15 hp (11.2 kW) blower.

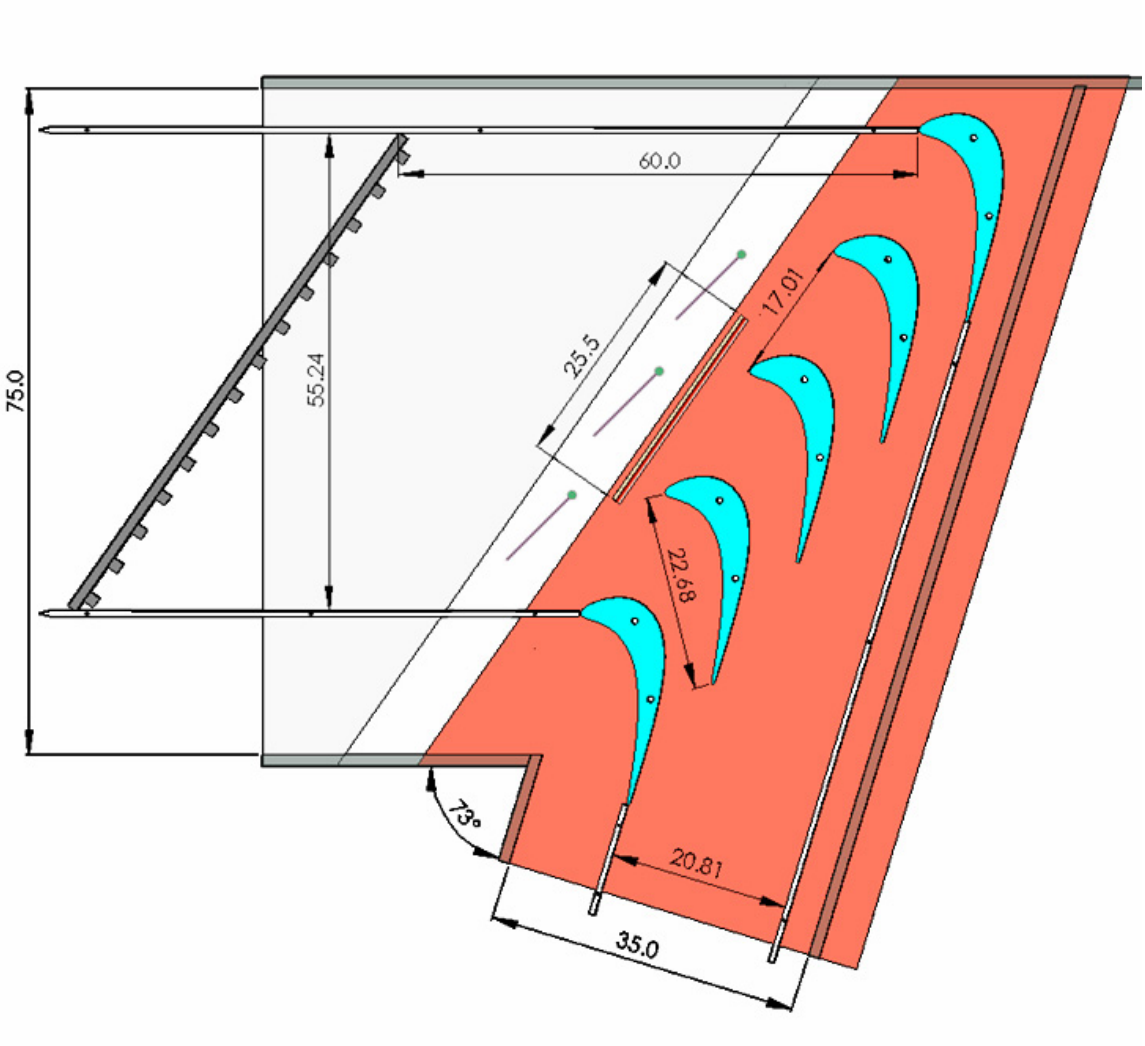

Figure 2: Detail of Low Speed Wind Tunnel and Turbine Blade Cascade

The mainstream air velocity at the cascade inlet was 20 m/s and the velocity at the outlet of the cascade was 50 m/s. The mainstream Reynolds number, based on inlet velocity and chord length, was $3.1*10^5$. In order to achieve a realistic background turbulence level of 5% at the cascade inlet, a turbulence grid was placed 60 cm upstream of the cascade leading edge. As measured by Zhang and Han [41] using hot-wire anemometry, the grid with 1.3 cm square bars spaced 4.8 cm apart creates a turbulence level of 5% with a length scale of 1.5 cm at the cascade inlet.

Linear Cascade

The linear cascade consists of five high pressure turbine blades scaled up five times. Each blade is 25.4 cm high with a chord length of 22.68 cm. The pitch between blades at the inlet is 17.01 cm. The inlet flow angle is 35° and the turning angle is 107.49°.

Stator-Rotor Seal

Coolant air or nitrogen was injected upstream of the cascade through a simulated stator-rotor seal. After passing through a square-edge ASME orifice flow meter, the coolant filled a plenum located beneath the platform. Then the coolant passed through the labyrinth-like seal as shown in Figure 3, turning 180° and exiting vertically. The seal has a length of 25.5 cm or 1.5 times the width of a single passage. The upstream edge of the final opening is vertical, while the downstream edge has a radius. To change the width of the seal opening, strips of foam tape were applied to the upstream vertical edge. The original width of the opening was 4.4 mm ± 0.2 mm. Tests were also performed with widths of 1.5 and 3.0 mm. For each width, tests were performed with coolant mass flow rates of 0.5%, 1.0%, 1.5%, and 2.0% of the mainstream mass flow rate.

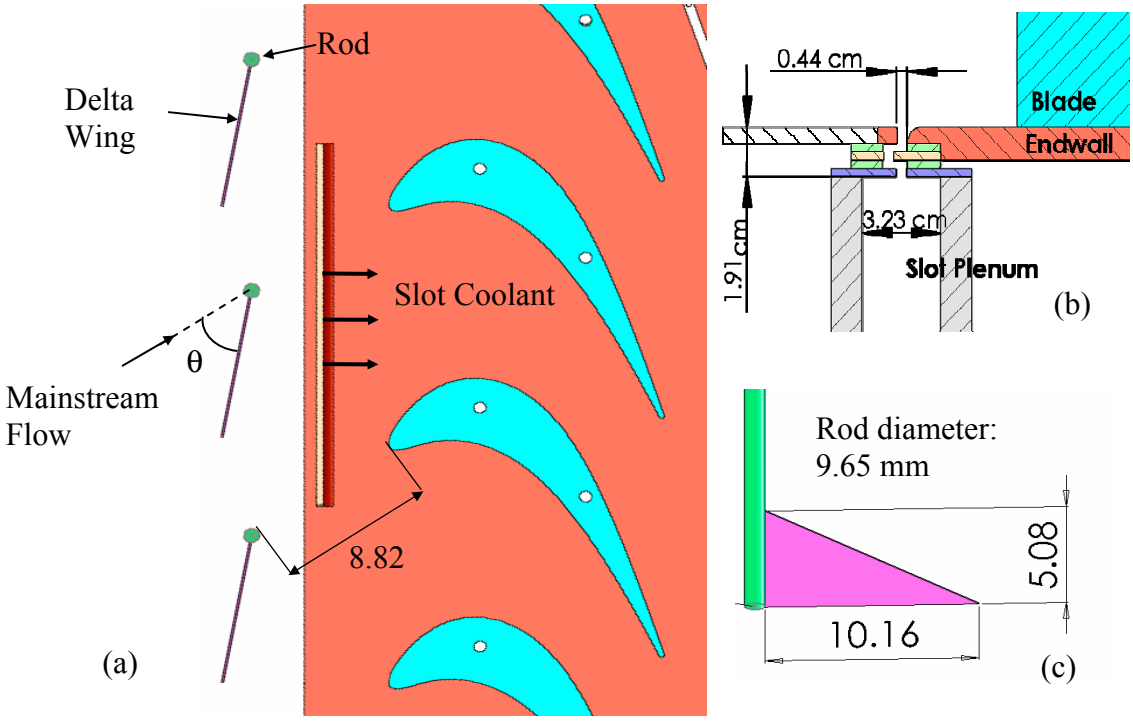

Figure 3: Platform Film Cooling Configuration (dimensions in cm) (a) Detail of Cooled Platform with Rod and Delta Wing, (b) Detail of Labyrinth-Like Stator-Rotor Seal, (c) Detail of Rod and Delta Wing

Upstream Wake and Vortex Generation

In order to determine the effect of the upstream wake, cylindrical rods were placed in the wind tunnel upstream of the blades. The rods are 9.65 mm in diameter and 25.4 cm long. The rods were placed 8.82 cm upstream of the blade leading edge in four positions as shown in Figure 4. The rod size and distance represents the largest of three sizes used by Han et al. [31] to approximate the trailing edge of the upstream vane. Since the effect of the rods was found to be minimal, tests were not repeated with the remaining two rods sizes used by Han et al. [31], 6.4 mm and 3.2 mm.

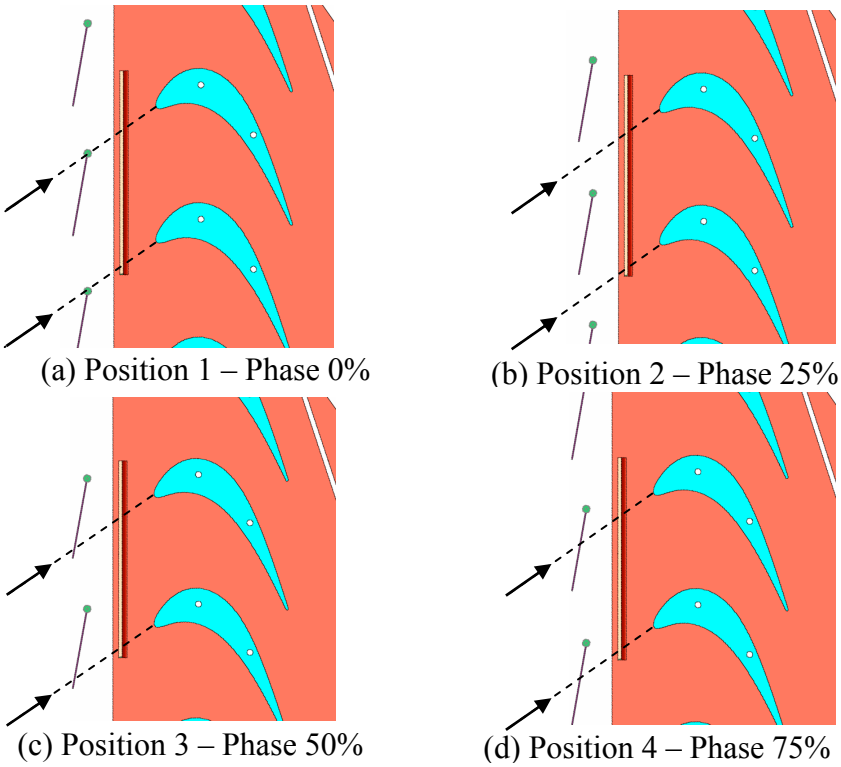

(a) Position 1 – Phase 0%

(b) Position 2 – Phase 25%

(c) Position 3 – Phase 50%

(d) Position 4 – Phase 75%

Figure 4: Rod and Delta Wing Positions In Reference to Stagnation Lines

Another goal of this study was to determine the effect of the passage vortex created in the upstream vane. This was accomplished by placing delta wings upstream of the blades, in the same four positions as the rods. The delta wings, as shown in Figure 3, are 5.08 cm high and 10.16 cm wide. Through CFD, these delta wings were found to produce a vortex, shown in Figure 5, similar in size to the passage vortex exiting the vane as measured by Hermanson [42]. The strength of the actual vane passage vortex corresponding to the blades in the cascade is difficult to predict, so the strength was varied by placing the delta wings at various angles to the mainstream flow. As the angle between the delta wing and the mainstream flow, θ, is increased the strength of the vortex is increased, while the size is relatively unchanged. Tests were performed with angles of 30° and 45°.

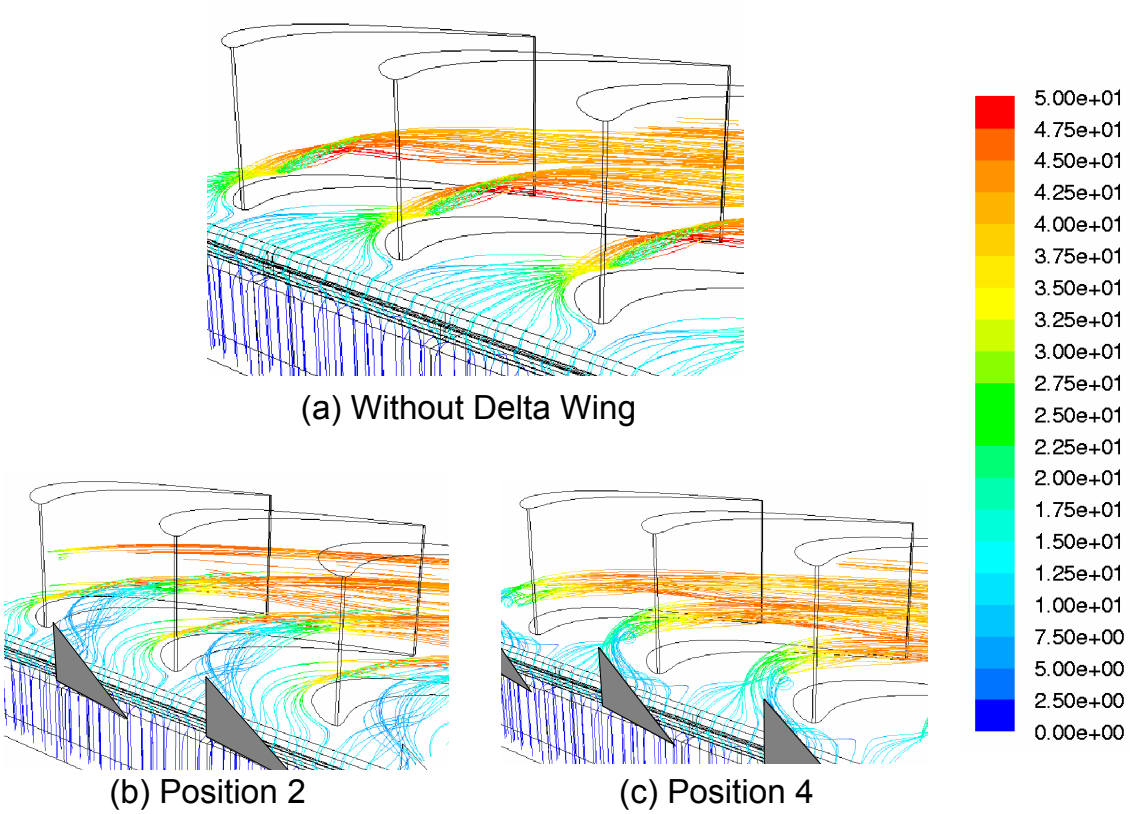

Figure 5: Flow in Cooled Passage (Path Lines Seeded near the Platform and Colored by Velocity Magnitude)

Tests were performed with both the rods and delta wings to determine the combined effect of the trailing edge wake and passage vortex from the vane. Tests with the rod and delta wing were performed with a seal width of 4.4 mm, and then tests were performed with widths of 1.5 mm and 3.0 mm, without rod or delta wing and with the delta wing at 45°.

Pressure-Sensitive Paint Measurement Technique

In each test, the film cooling effectiveness on the platform was measured using pressure-sensitive paint (PSP). PSP was first used to measure the film cooling effectiveness by Zhang et al. [24, 25]. Wright [43] compared this technique to steady state temperature-sensitive paint (TSP) and IR measurement techniques for measuring the film cooling

effectiveness on a flat plate. Gao [44] compared the steady-state PSP technique with a transient IR technique in a leading edge film cooling effectiveness study. Both studies found that the PSP results agreed well with heat transfer techniques and gave more accurate data near the film cooling holes, where the accuracy of heat transfer techniques suffers, due to conduction.

When excited by light of an appropriate wavelength, PSP emits light of a longer wavelength. The intensity of light emitted by the PSP depends on the partial pressure of oxygen in the air next to the painted surface. By measuring the intensity of the emitted light twice, once with air as a coolant, and once with nitrogen as a coolant, the film cooling effectiveness can be found as:

$$\eta = \frac{C_\infty - C_{mix}}{C_\infty} = \frac{\left(P_{O_2}\right)_{air} - \left(P_{O_2}\right)_{N2}}{\left(P_{O_2}\right)_{air}} \quad (1)$$

where C_∞ is the concentration of oxygen in air, C_{mix} is the concentration of oxygen in the mixture of air and nitrogen near the surface, $\left(P_{O_2}\right)_{air}$ is the partial pressure of oxygen in the air and $\left(P_{O_2}\right)_{N2}$ is the partial pressure of oxygen in the mixture of air and nitrogen near the surface.

First, the paint must be calibrated. A test plate sprayed with PSP was placed inside a vacuum chamber and exposed to a uniform reference pressure of atmospheric pressure. The intensity of light at this reference pressure was recorded. Next, a series of uniform pressures were applied, recording the intensity of the light at each pressure. Since the wind tunnel operates in suction and the use of nitrogen also decreases the partial pressure of oxygen during the tests, the calibration was performed for pressures less than atmospheric. From this data, a calibration curve was created to relate the ratio of the pressure at a data point to the reference pressure and the ratio of the intensity at the data point to the intensity at the reference pressure. This curve is shown in Figure 6.

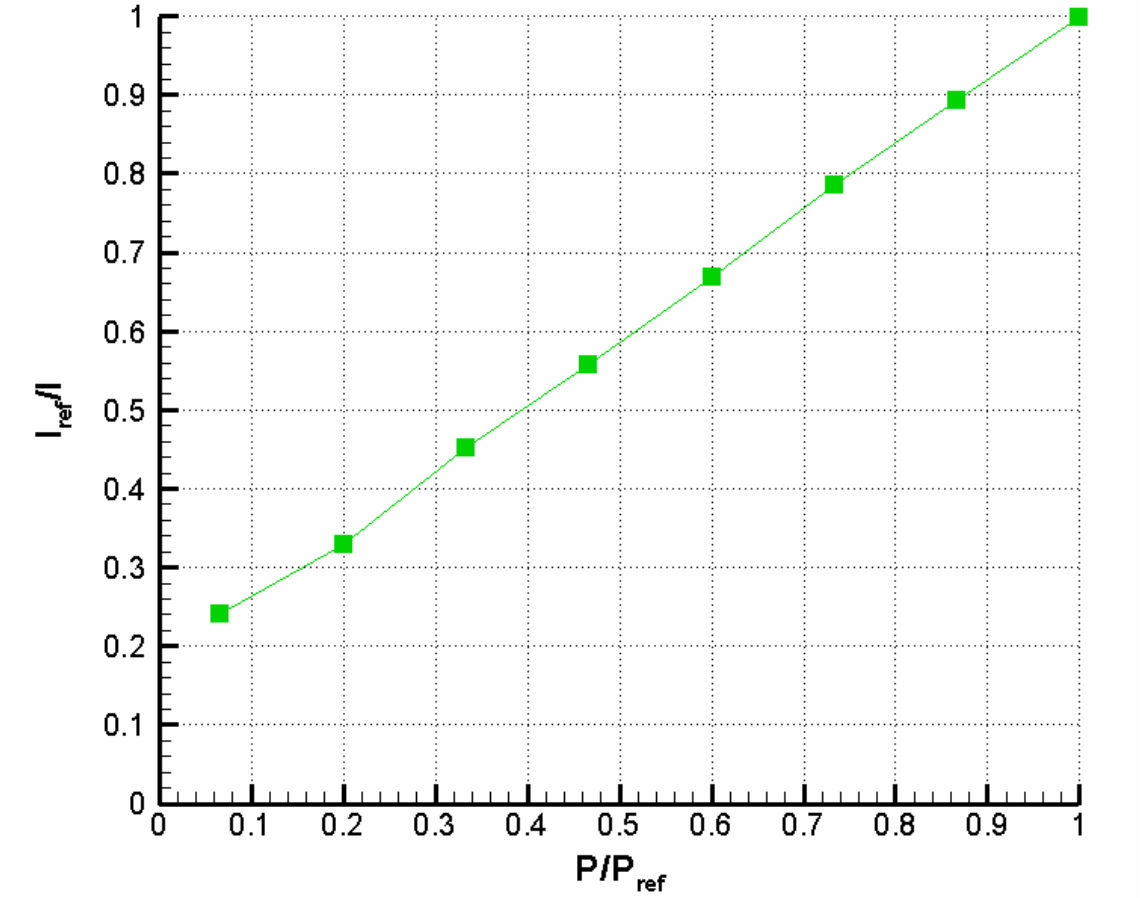

Figure 6: Calibration Curve for Pressure-Sensitive Paint Relating Intensity and Pressure Ratios

In order to determine the film cooling effectiveness, two test images were taken for each test condition. The first, the air image, was taken with mainstream and coolant flows of air. The second, the nitrogen image, was taken with a mainstream flow of air and a coolant flow of pure nitrogen. The mainstream and coolant flow rates were the same for the air image and the nitrogen image. Black and reference images, which were taken in still air at the reference pressure with and without light, were used to determine the

partial pressure of oxygen at any point in the air and nitrogen images. Then the film cooling effectiveness at each point was calculated as:

$$\eta = \frac{\left(P_{O_2}\right)_{air} - \left(P_{O_2}\right)_{N2}}{\left(P_{O_2}\right)_{air}} = \frac{f\left(\frac{I_{ref}}{I_{air}}\right) - f\left(\frac{I_{ref}}{I_{N2}}\right)}{f\left(\frac{I_{ref}}{I_{air}}\right)} \tag{2}$$

where $f\left(\frac{I_{ref}}{I}\right)$ is the pressure ratio found from the calibration curve at the intensity ratio $\frac{I_{ref}}{I}$.

Instrumentation

As shown in Figure 7, the velocity of the mainstream flow was measured using a pitot-static tube and micromanometer. Before entering the plenum, the coolant mass flow rate was measured using an ASME square-edged orifice flow meter and a U-tube manometer. The pipe diameter was 2.0 inches, while the orifice diameter was 1.0 inch. A pressure gauge measured the pressure upstream of the orifice flow meter.

The paint was excited with a strobe light filtered to a wavelength of 520 nm (green). The intensity of the paint was recorded using a CCD camera filtered to record light above 630 nm (red). The uncertainty of the film cooling effectiveness using this equipment was determined by Wright et al. [28 - 30] to be less than 2% when the effectiveness is greater than 0.5. As the effectiveness decreases, the relative uncertainty increases, reaching 10% at an effectiveness of 0.07.

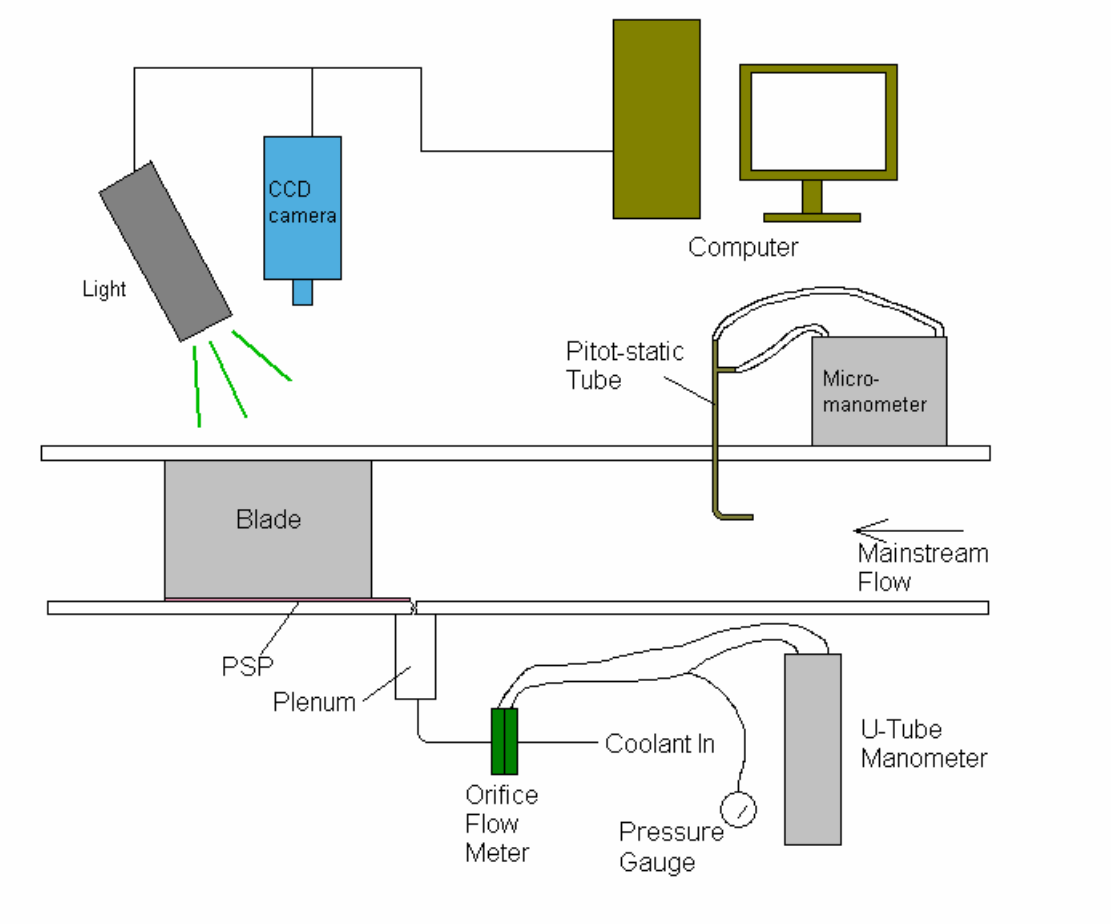

Figure 7: Experimental Setup and Instrumentation

RESULTS

Film cooling effectiveness distributions were obtained on the platform under the various conditions listed in Table 1. With the original slot width of 0.44 cm, tests were performed with stationary rods, with delta wings at two angles, and with both rods and delta wings, as well as without rods or delta wings. With slot widths of 0.30 cm and 0.15 cm, tests were performed with and without delta wings at 45°. In each case, the seal flow rate was varied from 0.5% to 2.0% of the mainstream mass flow rate, and if rods or delta wings were used, they were tested in four positions as shown in Figure 4. Selected detailed film cooling effectiveness distributions will be presented followed by comparisons of the laterally averaged film cooling effectiveness. Detailed effectiveness distributions for every case tested can be found in the appendix.

Table 1: Experimental Conditions

Slot Width, w (cm)	**Obstacles**	**Upstream Location**	**Seal Flow Rate, m_s**
0.44	None	-	0.5%, 1.0%, 1.5%, 2.0%
0.44	Rods	0%, 25%, 50%, 75%	0.5%, 1.0%, 1.5%, 2.0%
0.44	Delta Wings at 30°	0%, 25%, 50%, 75%	0.5%, 1.0%, 1.5%, 2.0%
0.44	Delta Wings at 45°	0%, 25%, 50%, 75%	0.5%, 1.0%, 1.5%, 2.0%
0.44	Rods and Delta Wings at 30°	0%, 25%, 50%, 75%	0.5%, 1.0%, 1.5%, 2.0%
0.44	Rods and Delta Wings at 45°	0%, 25%, 50%, 75%	0.5%, 1.0%, 1.5%, 2.0%
0.30	None	-	0.5%, 1.0%, 1.5%, 2.0%
0.30	Delta Wings at 45°	0%, 25%, 50%, 75%	0.5%, 1.0%, 1.5%, 2.0%
0.15	None	-	0.5%, 1.0%, 1.5%, 2.0%
0.15	Delta Wings at 45°	0%, 25%, 50%, 75%	0.5%, 1.0%, 1.5%, 2.0%

Baseline Case

In order to determine the effect of the upstream vane on rotor platform film cooling, the film cooling effectiveness distributions with simulated upstream vane conditions must be compared to some baseline case. Figure 8 shows the film cooling effectiveness distributions obtained with four coolant mass flow rates with a turbulence intensity of 5%. As was found in previous studies [3, 4], the film cooling effectiveness generally increases as the mass flow rate of the coolant is increased. With a flow rate of m_s = 0.5%, the film cooling effectiveness close to the slot is quite high, but it decreases

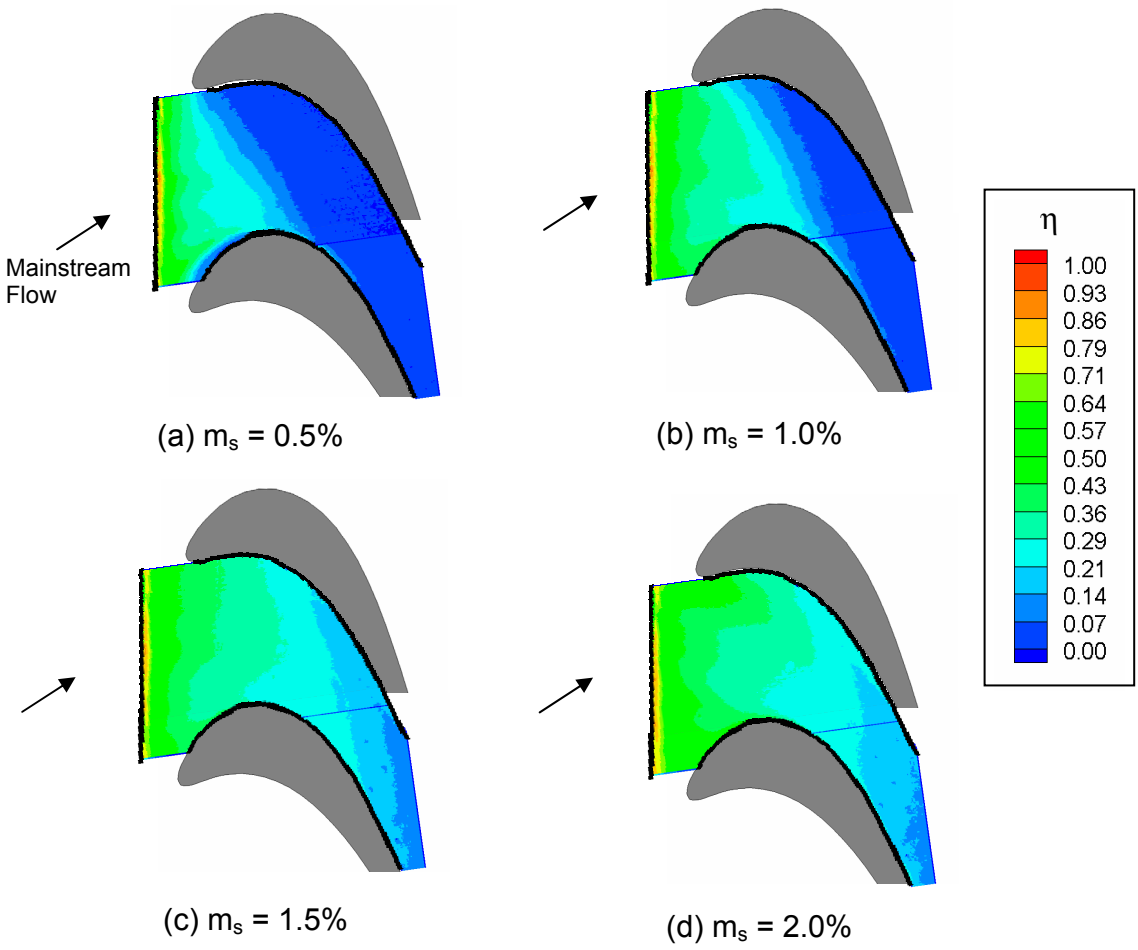

Figure 8: Film Cooling Effectiveness on Platform with Freestream Turbulence of 5%, w = 4.4 mm and Various Seal Injection Rates

quickly downstream, and most of the platform area receives little or no coolant. As the passage vortex moves from the pressure side of the passage to the suction side, it lifts the coolant off the platform. With a flow rate of 1.0%, the coverage is slightly improved. For higher flow rates of 1.5 and 2.0%, most of the platform is covered by the coolant. Unlike the lower flow rate cases, the coverage is quite even across the passage, indicating that the secondary flows have been reduced. It is likely that the coolant energizes the boundary layer and prevents the formation of the horseshoe vortex. There is only a small increase in coverage as the flow rate increases from 1.5 to 2.0%.

Stationary Rods

Figure 9 shows the film cooling effectiveness distributions on the platform with the addition of stationary rods with a coolant flow rate of 1.0%. In Figure 9a, the rods are aligned with the leading edges of the blades. When compared to Figure 8b, the addition of the rods gives slightly better coverage in the downstream portion of the passage, but the distribution in the upstream portion is slightly lower. It appears that the wake from the rods disrupts the formation of the horseshoe vortex, slightly weakening the passage vortex, such that the coolant is not swept toward the suctions side as quickly.

With the rod in the other three positions, the effect of the rod is even smaller. In Figure 9b, when the rod is in Position 2, the wake also reduces the passage vortex. With the rod in Positions 3 and 4, the wake is in the center of the passage and doesn't influence the formation of the horseshoe vortex, so the film cooling effectiveness is nearly identical to the baseline case.

It might be expected that the effectiveness directly downstream of the rod would be affected by the wake. However, the path of the wake is not apparent in the distributions, suggesting that the flow is dominated by the ejection of coolant from the slot, and the

wake from the rod does not contact the surface. Similar trends were observed for other mass flow rates.

Delta Wings

When delta wings were placed upstream of the blades at an angle of 30° from the mainstream, the effect was slightly more noticeable than that of the rods, as shown in Figure 10. In Figure 10a, the vertical edge of the delta wing is aligned with the leading edge of the blade. The coolant coverage is reduced, especially near the leading edge of

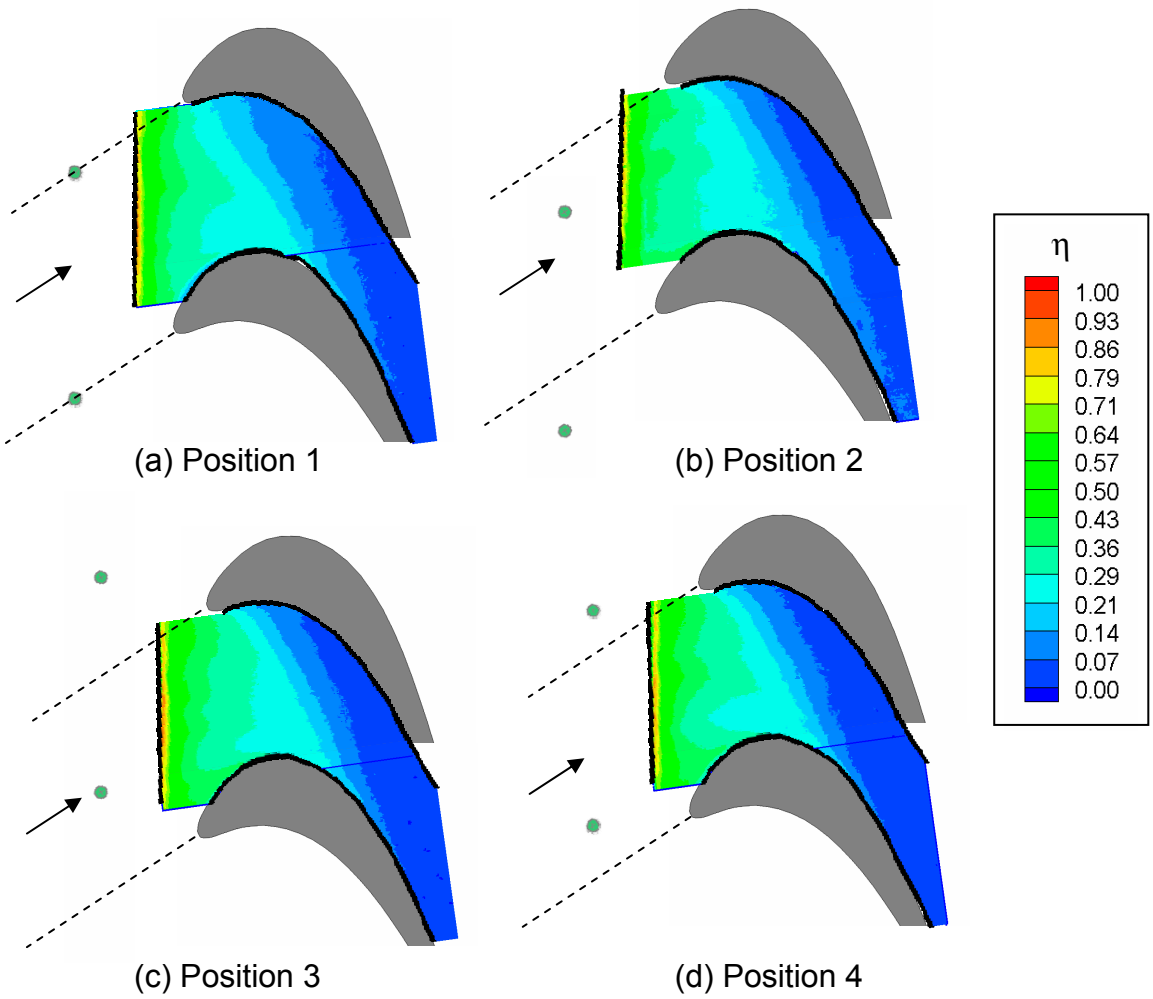

Figure 9: Film Cooling Effectiveness on Platform with Wake Rod in Four Positions and m_s = 1.0%

the blades, suggesting that the horseshoe vortex on the suction side of the blade is stronger than without the delta wing. Also, on the suction side near the leading edge of the blade, the effectiveness is low, as in Figure 8a, due to the horseshoe vortex.

With the delta wings in Position 2, the effectiveness directly downstream of the delta wing is reduced. The vortex lifts the coolant in its path off of the surface. In general, the effectiveness is slightly lower than without the delta wing. With the delta wings in Positions 3 and 4, there is no noticeable change from the baseline case, except that for

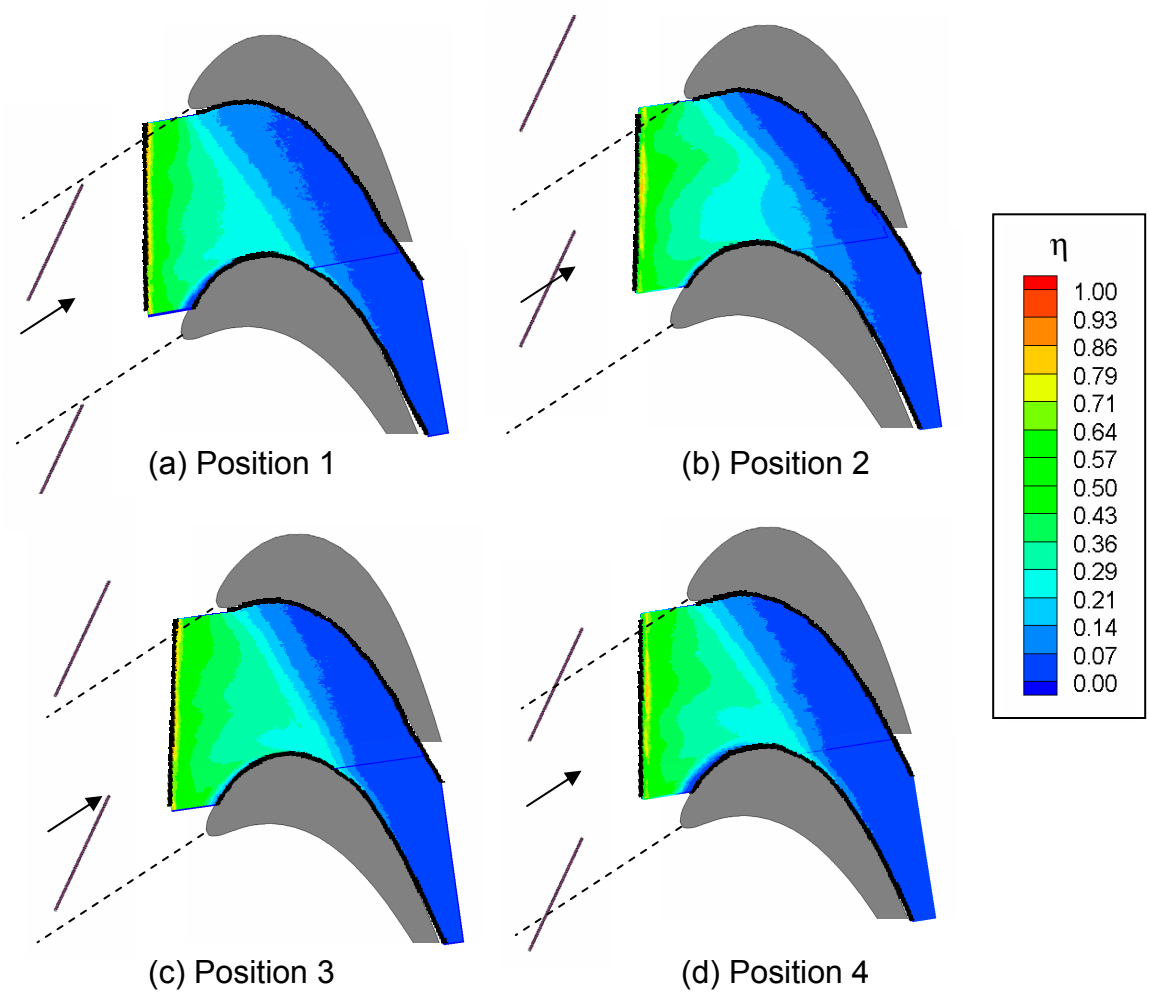

Figure 10: Film Cooling Effectiveness on Platform with Delta Wing in Four Positions, m_s = 1.0% and θ = 30°

Position 4, there is again an area of very low effectiveness near the suction side of the leading edge of the blade.

When the delta wings are placed at an angle of 45° to the mainstream flow, the film cooling effectiveness distributions change drastically, as shown in Figure 11. In Position 1, the delta wing significantly reduces the film cooling effectiveness, especially in the pressure-side half of the passage, directly downstream of the delta wing. In Position 2, the effectiveness directly downstream of the delta wing is reduced, but in general, the

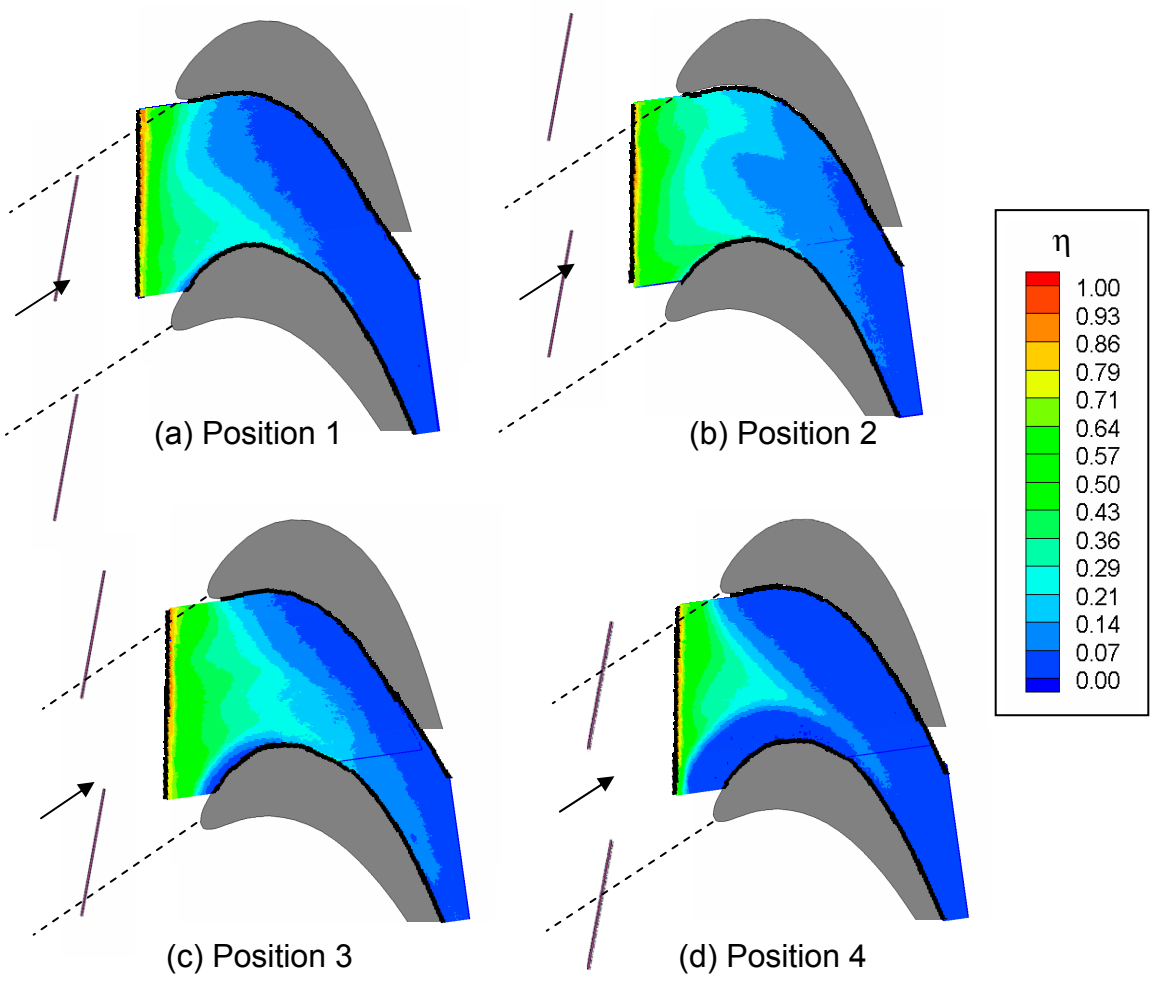

Figure 11: Film Cooling Effectiveness on Platform with Delta Wing in Four Positions, $m_s = 1.0\%$ and $\theta = 45°$

effectiveness is increased, and coverage extends farther downstream than when no delta wing is present. It appears that the vortex from the delta wing disrupts the formation of the passage vortex. With the delta wing in Position 3, the delta wing vortex apparently increases the strength of the suction-side leg of the horseshoe vortex, preventing any coolant from covering the area near the suction side of the leading edge. However, farther downstream the delta wing vortex appears to push the coolant farther along the surface, giving higher effectiveness values. Finally, in Position 4, the delta wing vortex is directly aligned with the blade leading edge and increases the strength of both legs of the horseshoe vortex, removing the coolant from most of the passage. In fact, the coverage is even less than in Figure 8a, where the coolant flow rate was 0.5% or half as much as in Figure 11.

It is clear that the passage vortex from the upstream vane can significantly affect rotor platform cooling and that this factor should be considered in cooling designs. However, the importance of the vane passage vortex depends greatly on its strength, which varies with vane geometry and flow conditions. Therefore, it can not be assumed that the effect will be as significant as that shown in Figure 11. When designing turbine platform cooling, it is necessary to consider the strength of the passage vortex in the corresponding vane.

Rods and Delta Wings

In an actual turbine, the rotor is subjected to both the unsteady wake and the passage vortex from the upstream vane, so it is important to consider the combined effect. Though the wake rods alone were shown to have little impact on the film cooling, it was important to see whether the presence of the wake rods would impact the delta wing vortex. The wake rods and delta wings were placed together upstream of the vane. The results were found to be nearly identical to the results with delta wing only, as shown in Figure 12. Figure 12 shows the effectiveness distributions with both the wake rod and the delta wing at an angle of 45°, and the distributions are essentially the same as in

Figure 11. Similarly, with the delta wing at 30° and the wake rod, the results were very similar to Figure 10.

Figure 13 shows the effectiveness distributions with the wake rods and the delta wings at 45° for various coolant flow rates, with the rods and delta wings in Position 4. When comparing Figures 8 and 13, it is apparent that the delta wings significantly affect the

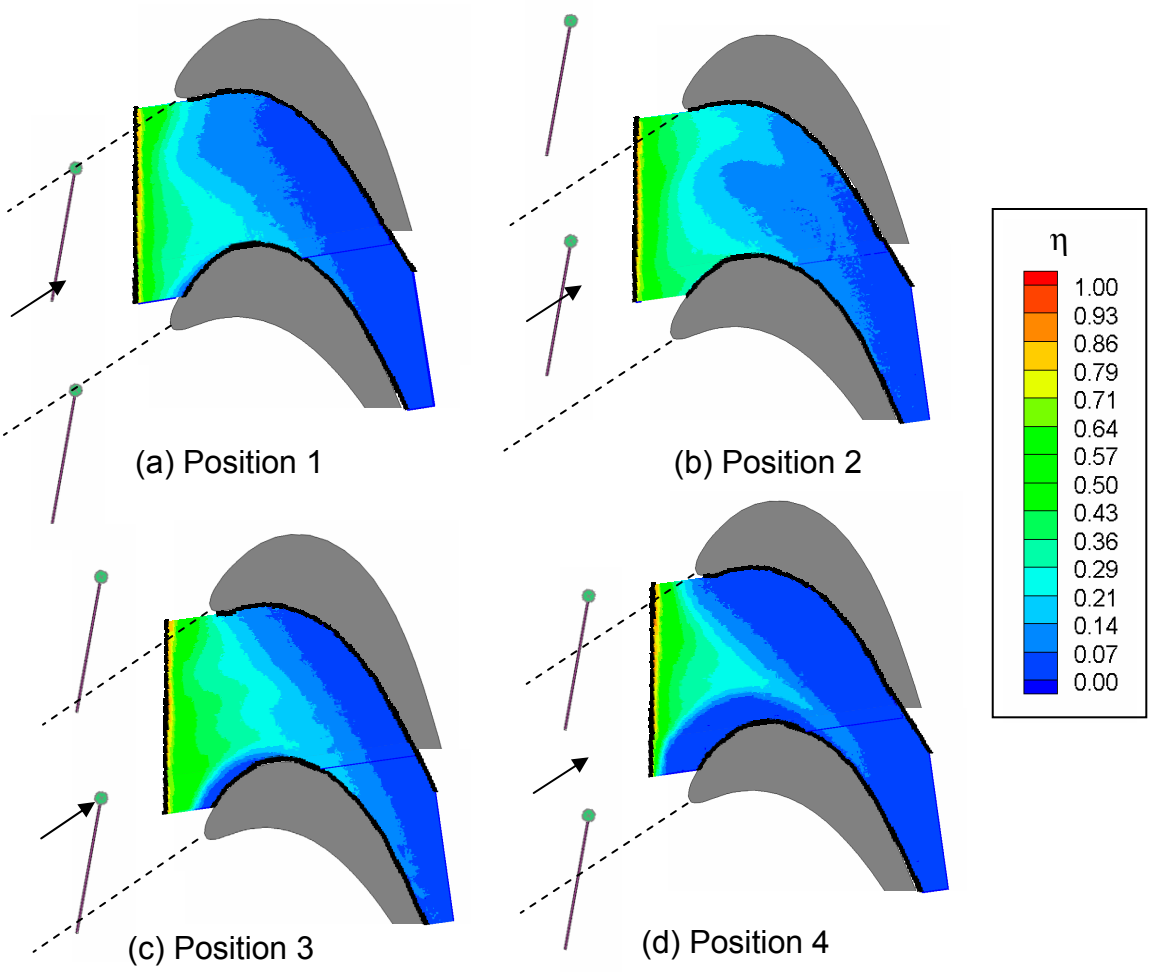

Figure 12: Film Cooling Effectiveness on Platform with Wake Rod and Delta Wing in Four Positions, m_s = 1.0% and θ = 45°

film cooling effectiveness at every coolant flow rate. Even with the highest flow rate of m_s = 2.0%, the coverage is significantly reduced.

Varied Seal Width

In a real engine, the width of the stator-rotor seal depends on the alignment of the stator and rotor. Variations with temperature and use may cause the seal width to change, affecting the flow rate and momentum of the coolant ejected through the seal. As the seal width decreases for the same coolant flow rate, the momentum of the coolant increases.

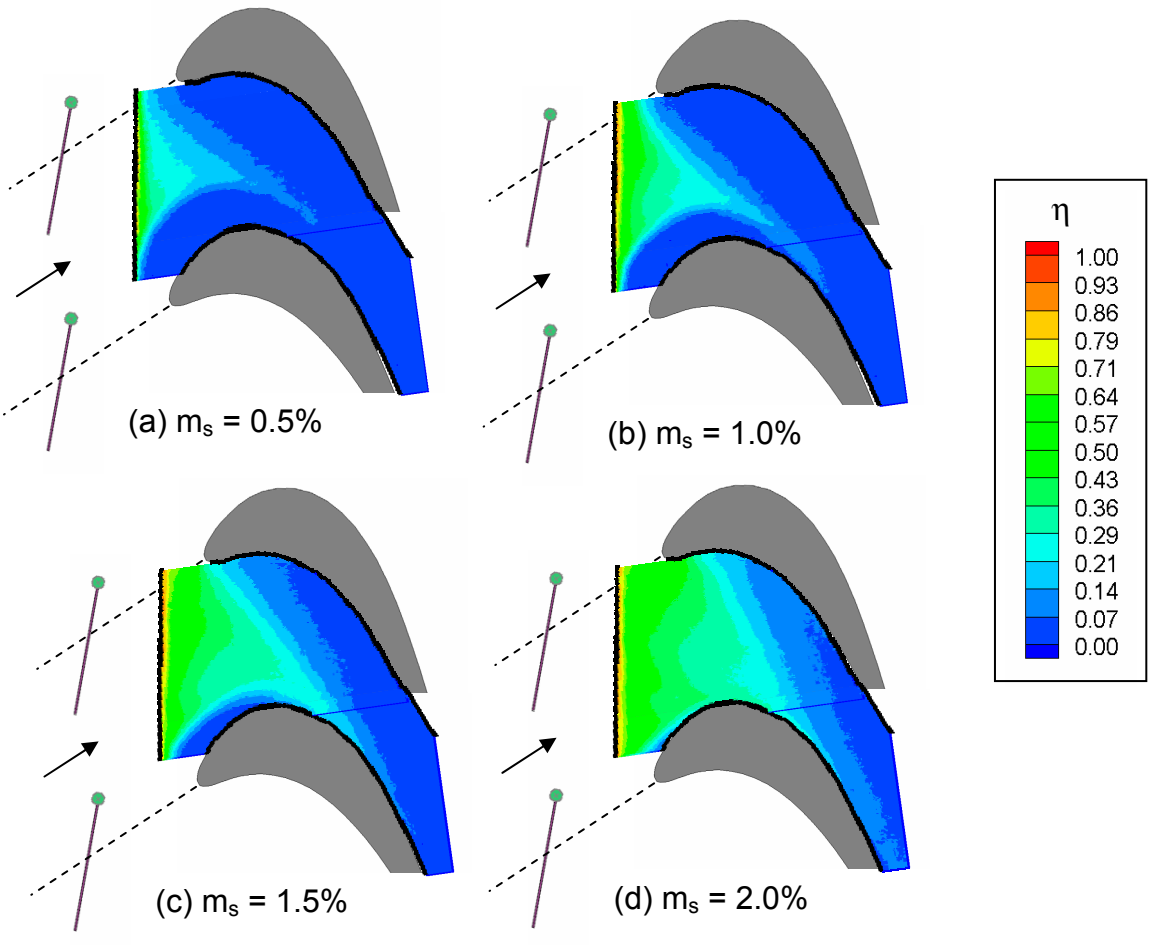

Figure 13: Film Cooling Effectiveness on Platform with Wake Rod and Delta Wing in Position 4, θ = 45° and Various Seal Injection Rates

To study this effect, the 4.4 mm slot in the test facility was reduced to 3.0 mm and finally 1.5 mm. Table 2 lists the four blowing rates tested for each slot width, along with the corresponding blowing ratio, a ratio of the coolant and mainstream momentums. Figure 14 shows the film cooling effectiveness distributions on the platform with a 3.0 mm slot width and no wake rod or delta wing. The results are similar to Figure 8, but the coverage is more uneven. However, the effectiveness close to the slot is increased.

When the slot width is further reduced to 1.5 mm, the same trends continue, as shown in Figure 15. The effectiveness close to the slot is noticeably higher, but downstream, the effectiveness is less, especially on the pressure side. A coolant flow rate of 1.5% covers approximately the same area as a coolant flow rate of 1.0% with the 4.4 mm slot width. For a coolant flow rate of 2.0%, the effectiveness along the pressure side is much lower than for the larger slot widths, but the coolant is pushed much farther along the suction side. This suggests that the secondary flows in the passage are increased by the high momentum coolant. As indicated in Table 2, the blowing ratios for the 1.5 mm slot ranged from 0.85 to 3.34, meaning the momentum is very high for film cooling.

Table 2: Blowing Rates and Blowing Ratios

Slot Width (mm)	Blowing Ratio (M_s)			
	m_s = 0.5%	m_s = 1.0%	m_s = 1.5%	m_s = 2.0%
4.4	0.29	0.57	0.86	1.14
3.0	0.43	0.84	1.26	1.67
1.5	0.85	1.67	2.52	3.34

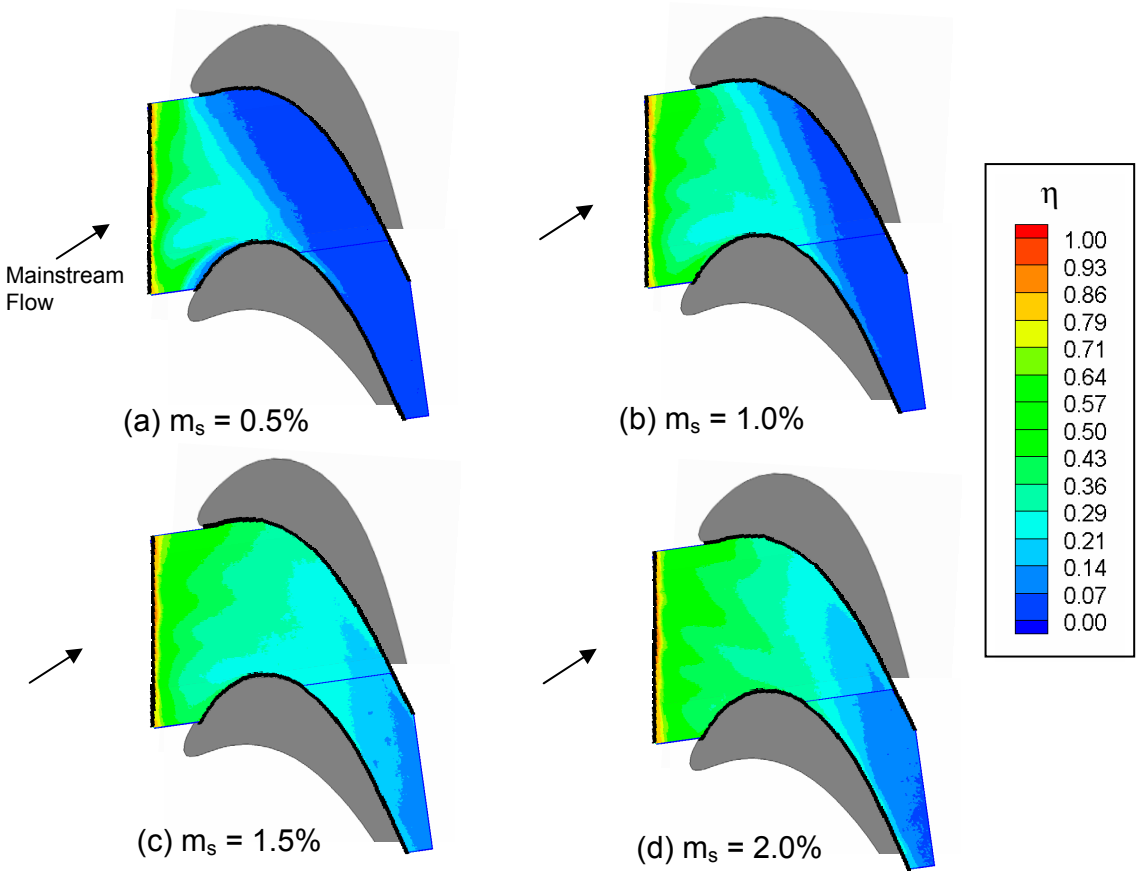

Figure 14: Film Cooling Effectiveness on Platform with Freestream Turbulence of 5%, w = 0.30 cm and Various Seal Injection Rates

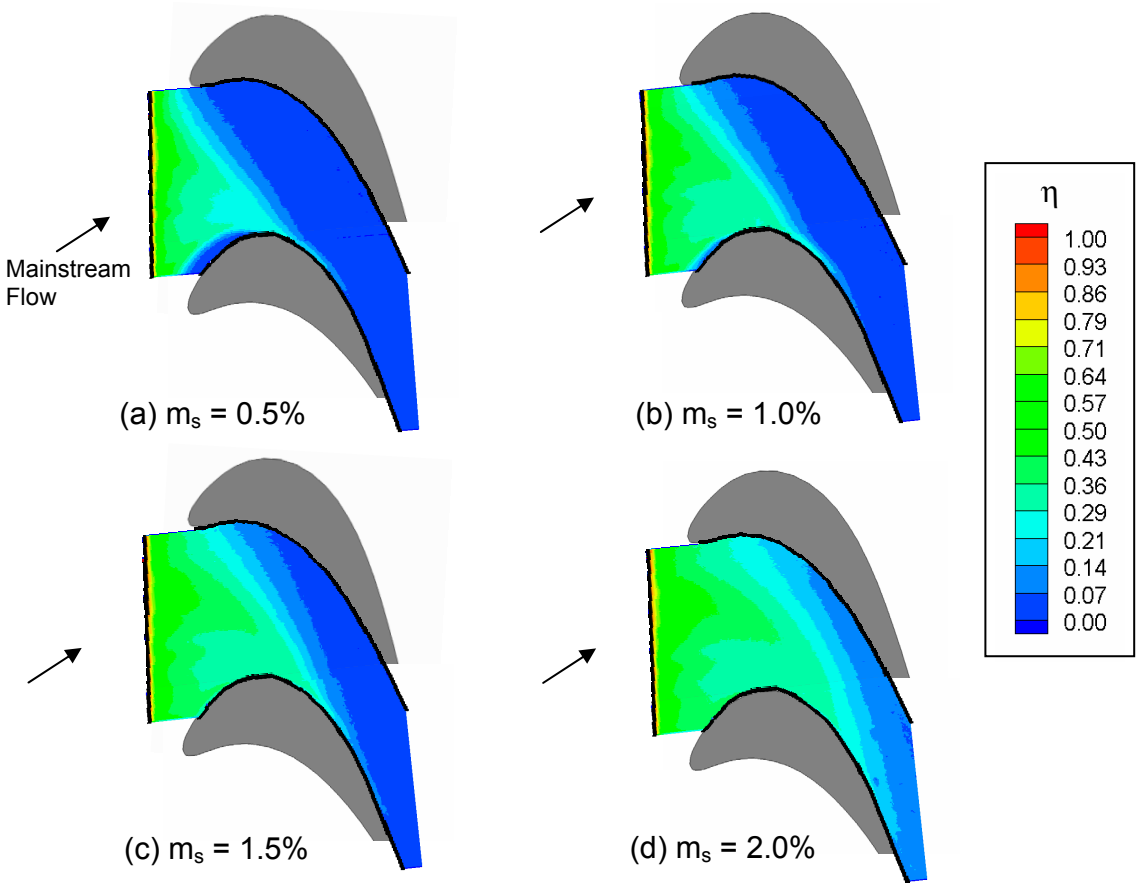

Figure 15: Film Cooling Effectiveness on Platform with Freestream Turbulence of 5%, w = 0.15 cm and Various Seal Injection Rates

Figure 16 illustrates the effect of the upstream vane passage vortex with a reduced seal width. The delta wings are placed at 45° in four positions as in Figure 12, but the seal width is 3.0 mm instead of 4.4 mm. The effect of reducing the seal width is striking. The increased coolant momentum combined with the delta wing vortex apparently leads to very high mixing between the coolant and mainstream. For each position, the coolant coverage is significantly less than in Figure 12. In Figure 16d, with the delta wing in Position 4, only a small portion of the passage is covered by the coolant, mostly upstream of the blades.

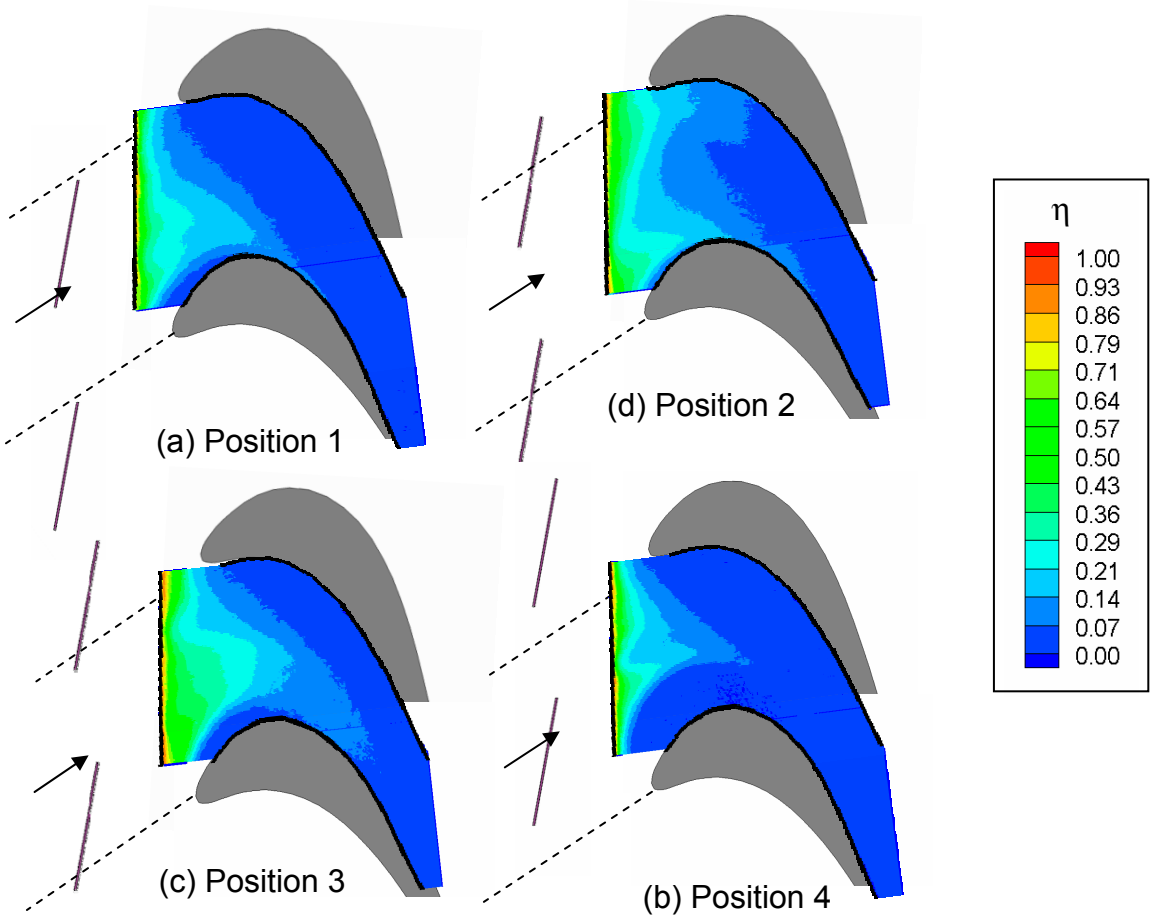

Figure 16: Film Cooling Effectiveness on Platform with Delta Wing in Four Positions, m_s = 1.0%, θ = 45° and w = 0.30 cm

As compared to Figure 14b, where the slot width is also 3.0mm, but no delta wing is present, the effectiveness in Figure 16 is very low. For the slot width of 4.4 mm and m_s = 1.0%, it was seen that the delta wing in Position 2 decreased the effectiveness in the upstream portion, but extended coverage farther downstream. For the slot width of 3.0 mm, this is not the case. The delta wing, even in Position 2, decreases the effectiveness throughout the passage.

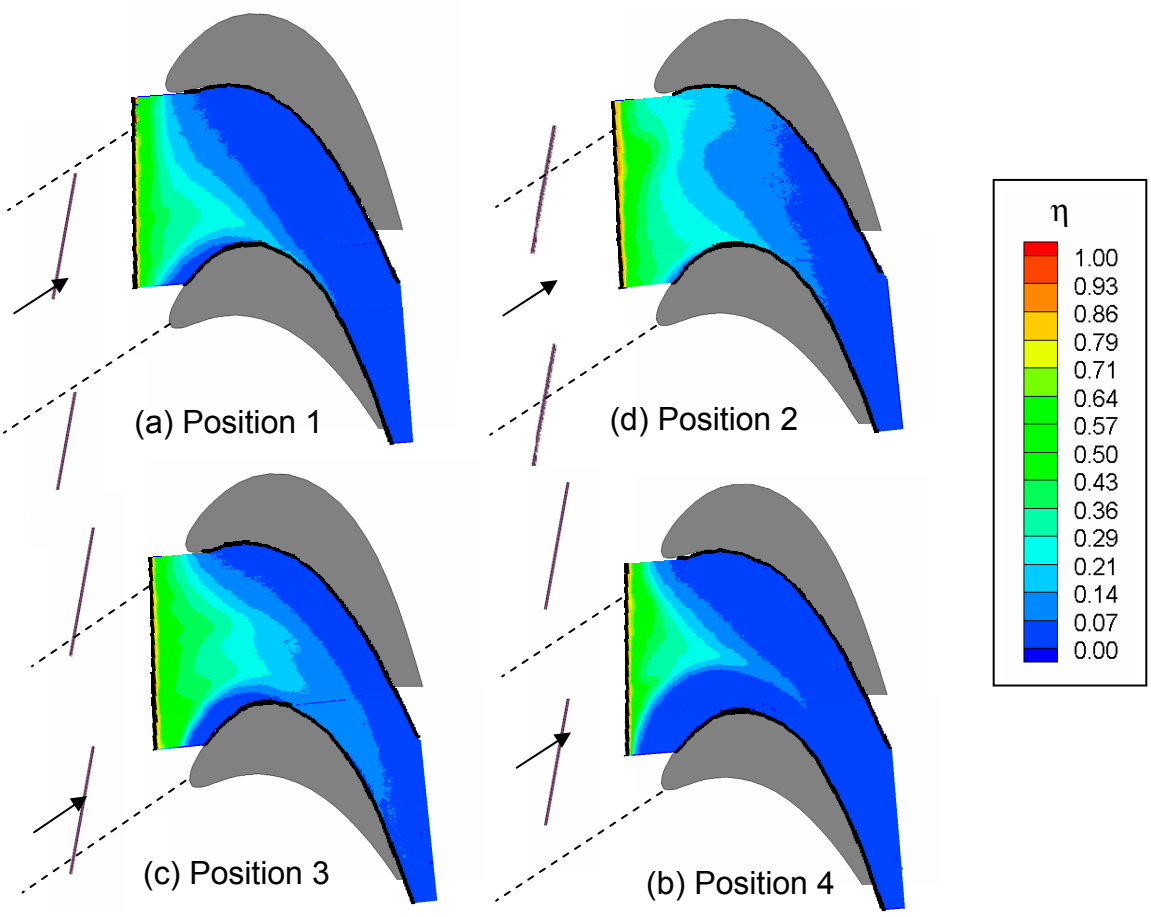

Figure 17: Film Cooling Effectiveness on Platform with Delta Wing in Four Positions, m_s = 1.0%, θ = 45° and w = 0.15cm

In Figure 17, the seal width is 1.5mm, and the delta wings are placed at 45°. The area of coverage is similar to that for the 3.0mm slot in Figure 16, but the effectiveness is slightly higher. The increased momentum keeps more of the coolant close to the surface, but the coolant is still mixed into the mainstream relatively quickly as compared to Figure 11.

Again, the delta wing effect is very strong for the 1.5mm slot. The effectiveness is much lower than in Figure 15b, although for Position 2, the effectiveness extends slightly farther downstream.

Laterally Averaged Film Cooling Effectiveness

In order to compare various cases quantitatively, the film cooling effectiveness was averaged across the passage. The results for the 4.4mm slot and $m_s = 0.5\%$ are shown in Figure 18. The solid black line in each plot represents the results for w = 4.4 mm, m_s = 0.5%, and no upstream obstacles. The quantity x/C_{ax} represents the distance from the leading edge of the blade, where values less than zero indicate a position upstream of the blade and a value of one indicates the trailing edge plane. In each position, the results for the rod alone, the delta wing at 30°, and the rod with delta wing at 30° are quite close to the baseline case. However, for positions 1, 3, and 4, both cases with the delta wing at 45° (green squares and black diamonds) give significantly lower effectiveness upstream of the leading edge and downstream to half the axial chord length. In the downstream half of the passage, the effectiveness is less than 0.1 for all cases, but it is slightly higher for the delta wings in Position 2 than for other cases.

With the coolant flow rate increased to 1.0%, the effect of the delta wings is shifted downstream, as seen in Figure 19. Very close to the slot, the effectiveness is nearly the same for all cases, but for x/Cax between -0.1 and 0.5, the effectiveness with the delta wings at 45° is considerably lower than with other cases. The strongest effect is with the

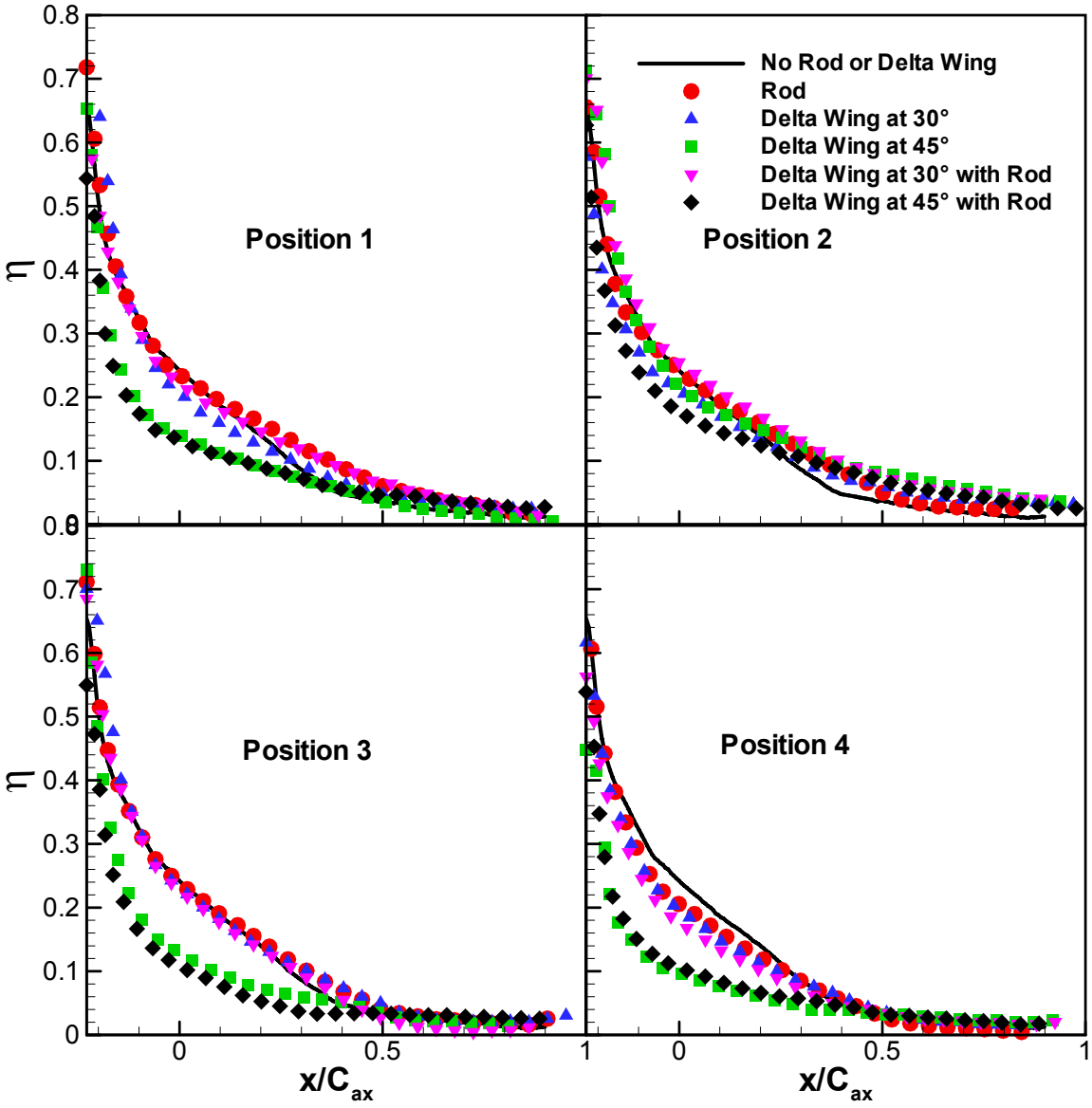

Figure 18: Comparison of Laterally Averaged Film Cooling Effectiveness on the Platform for Various Upstream Conditions, m_s = 0.5% and w = 4.4 mm

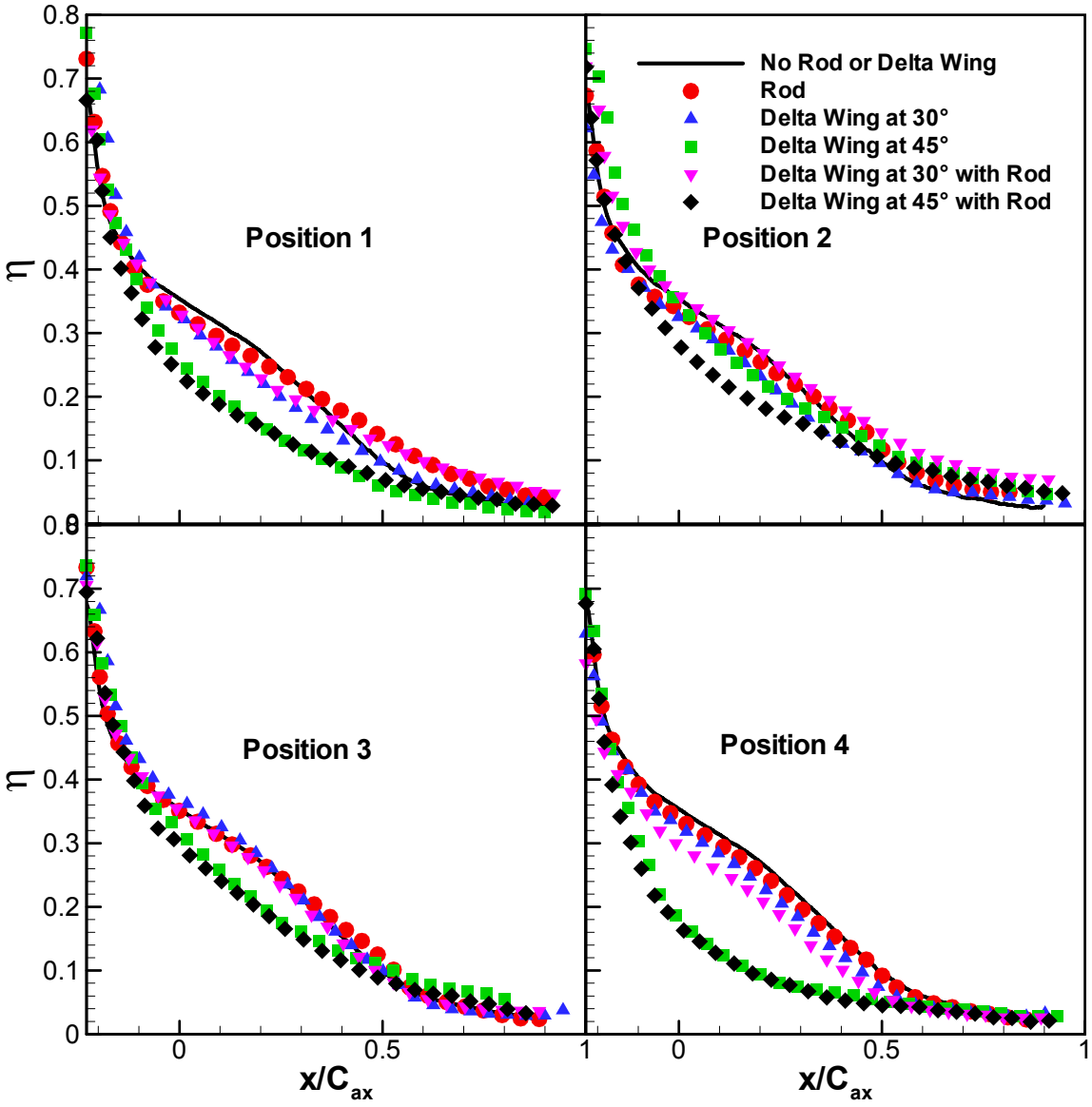

Figure 19: Comparison of Laterally Averaged Film Cooling Effectiveness on the Platform for Various Upstream Conditions, m_s = 1.0% and w = 4.4 mm

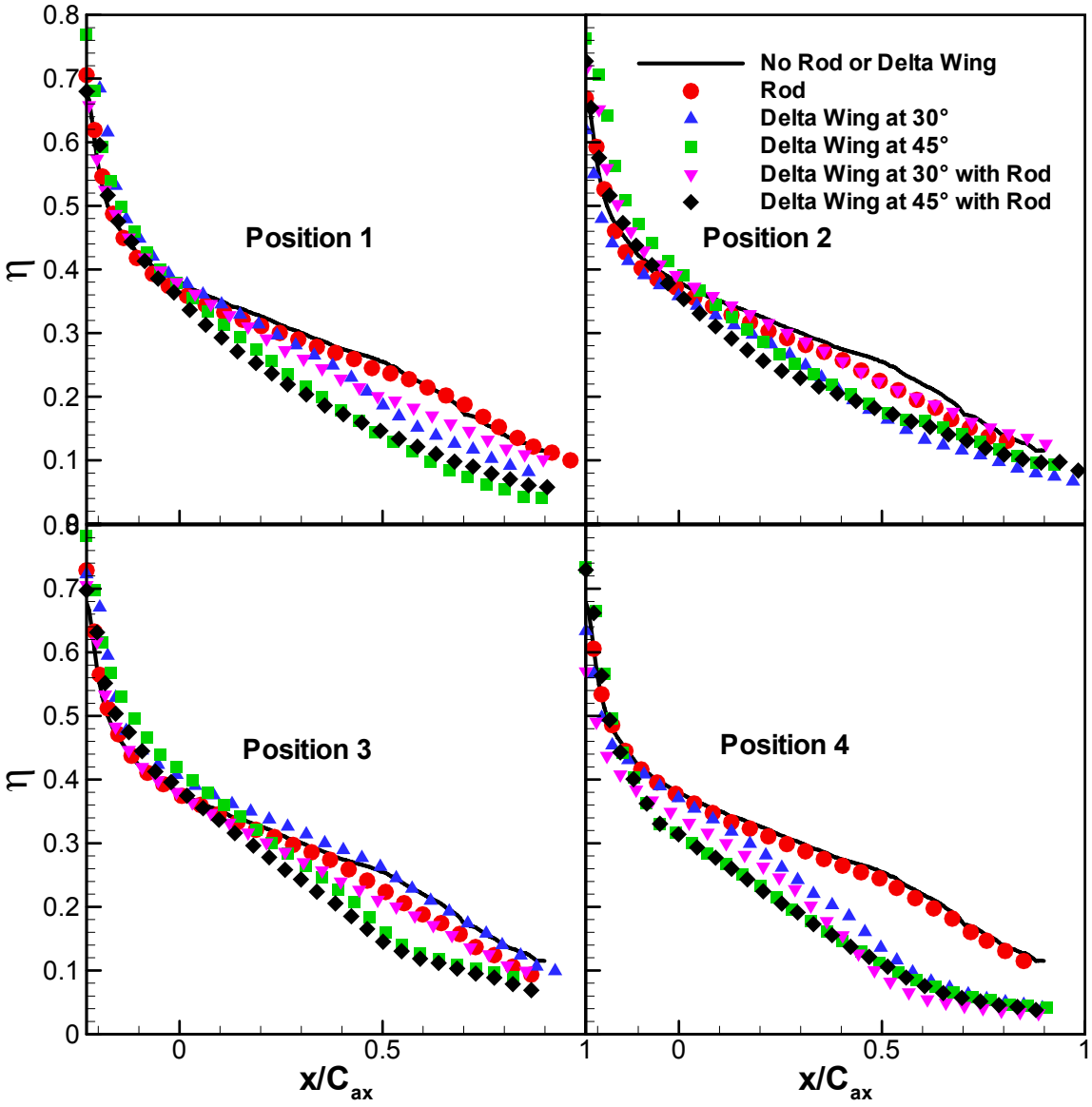

Figure 20: Comparison of Laterally Averaged Film Cooling Effectiveness on the Platform for Various Upstream Conditions, m_s = 1.5% and w = 4.4 mm

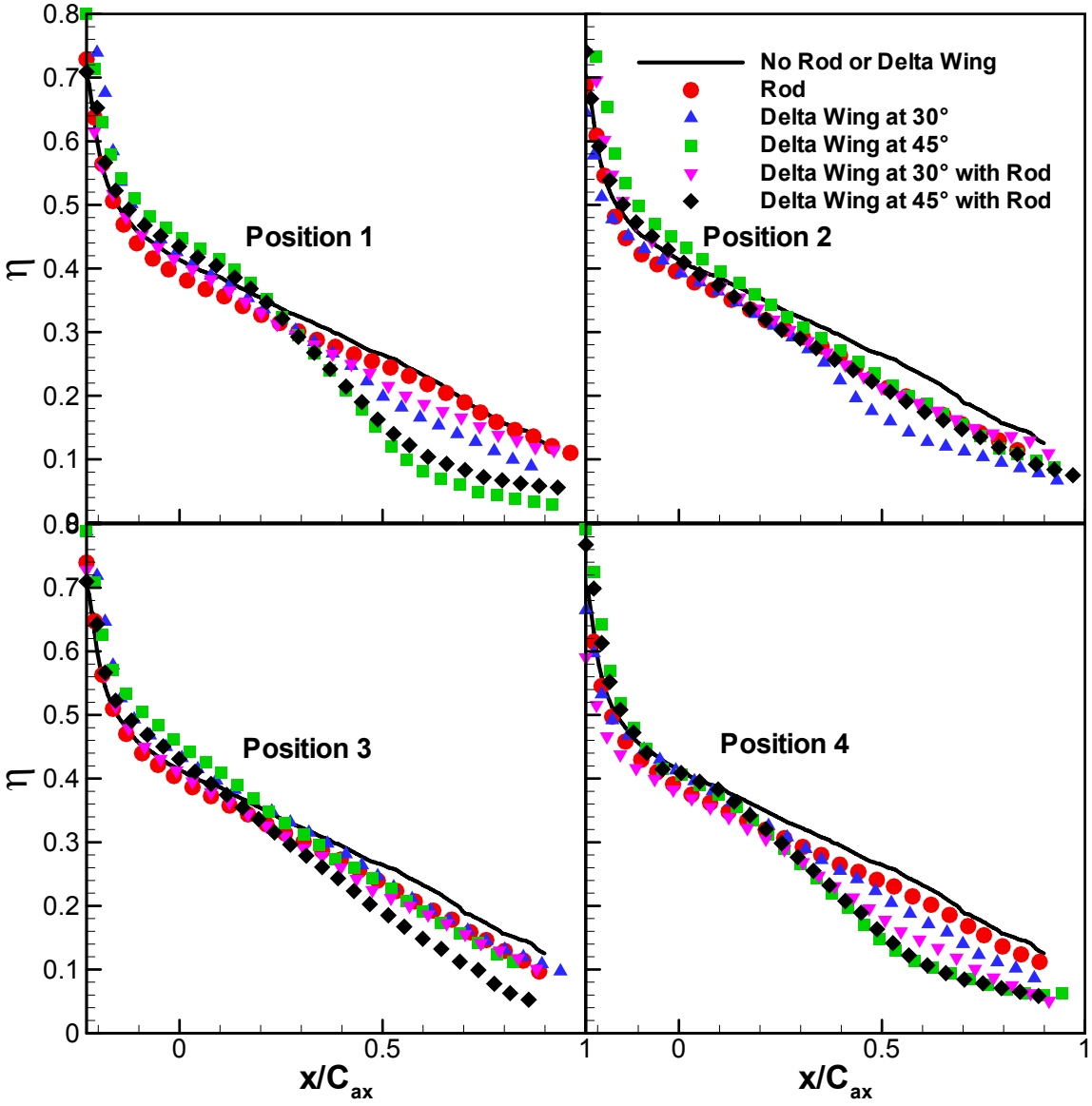

Figure 21: Comparison of Laterally Averaged Film Cooling Effectiveness on the Platform for Various Upstream Conditions, m_s = 2.0% and w = 4.4 mm

delta wings in Position 4. In this position, even the delta wings at 30° noticeably decrease the effectiveness.

When the coolant flow rate is further increased, the effect of the delta wings decreases, and the effect moves even farther downstream. In Figure 20, for m_s = 1.5%, there is little variation in effectiveness upstream of the leading edge, except in Position 4. However, the effect of the delta wings, especially in Positions 1 and 4, extends to the trailing edge. It is interesting to note that for Position 4, the effect of the delta wing at 30° is nearly as strong as at 45°, while the rod alone has no measurable effect.

At a coolant flow rate of m_s = 2.0%, as shown in Figure 21, the rods and delta wings have little effect before x/C_{ax} of 0.2. In the downstream portion of the passage, the effect is quite strong. For the baseline case, the effectiveness near the trailing edge is about 0.1, but with the delta wings at 45° in Position 1 or 4, the effectiveness is near zero.

Figure 22 shows the laterally averaged film cooling effectiveness for each of the three seal widths with a coolant flow rate of m_s = 0.5%. The closed symbols, which are the same in each plot, represent the effectiveness without delta wings. The open symbols represent the effectiveness with delta wings in each position. Without the delta wings, the effectiveness is higher for a slot width of 3.0 mm than 4.4 mm. For 1.5 mm, the effectiveness distribution is similar to 4.4 mm, but slightly higher near the slot. With the delta wings in Position 1, the effectiveness for all slot widths is lower than without the delta wings. However, the change in effectiveness is greater for the smaller slot widths, especially for 3.0 mm. This suggests that the delta wing vortex has more effect on the coolant flow when the slot is narrower. For the other positions, the delta wing effect is also strongest for the 3.0 mm slot. Whereas the delta wing in Position 2 had little effect on the 4.4 mm slot injection, it has a noticeable effect on the smaller slots.

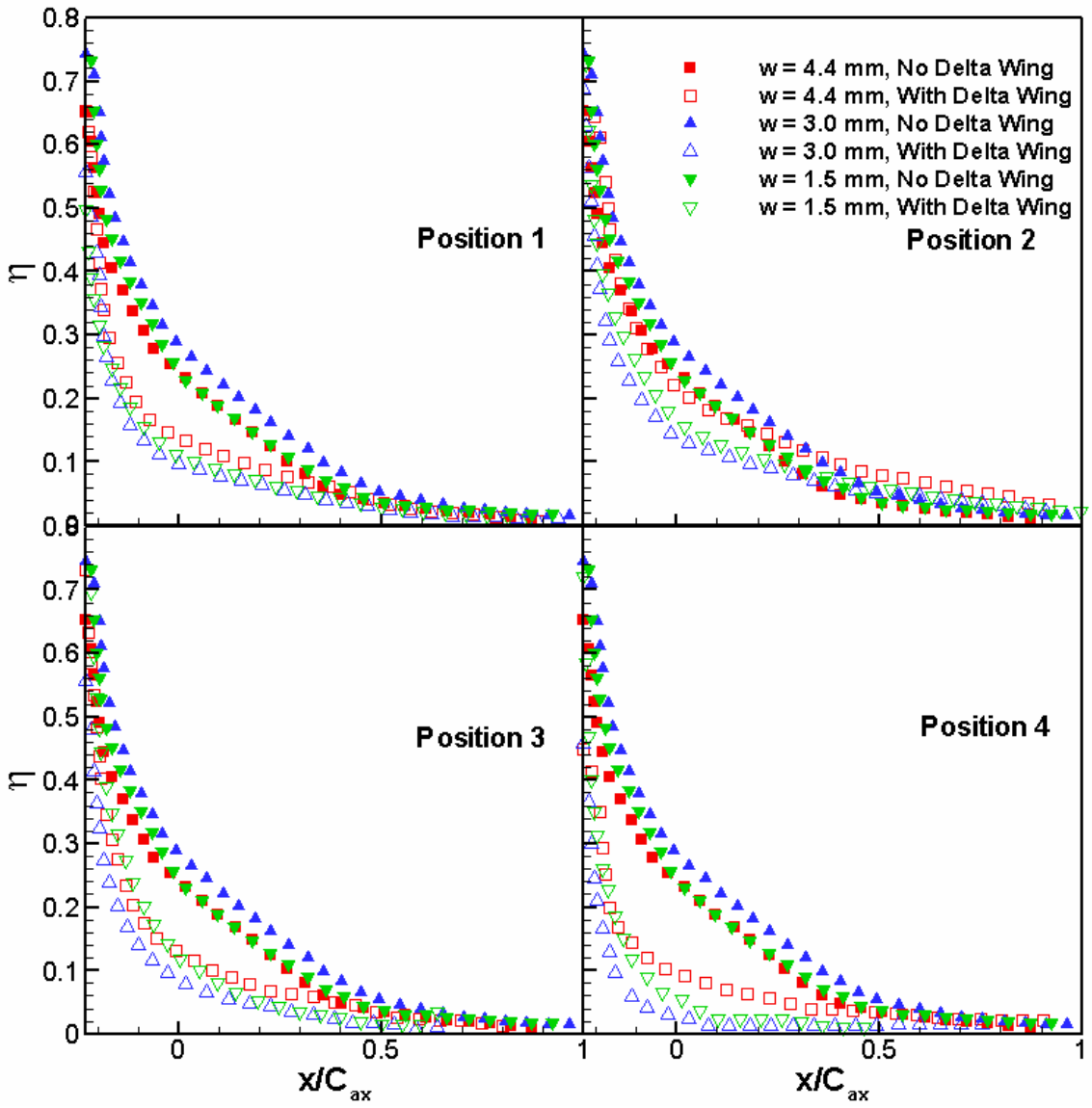

Figure 22: Comparison of Laterally Averaged Film Cooling Effectiveness on the Platform for Various Slot Widths, $\theta = 45°$ and $m_s = 0.5\%$

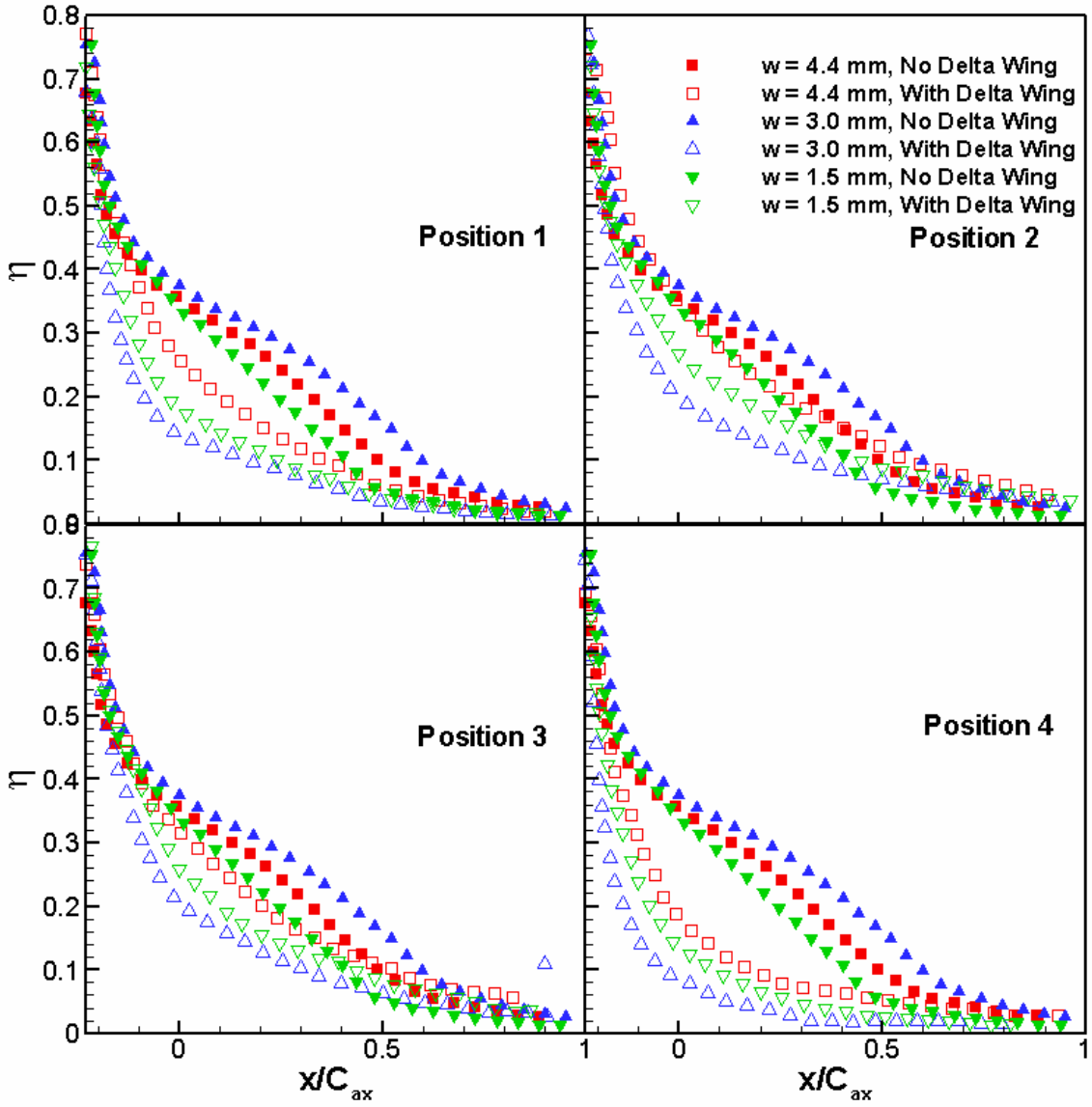

Figure 23: Comparison of Laterally Averaged Film Cooling Effectiveness on the Platform for Various Slot Widths, $\theta = 45°$ and $m_s = 1.0\%$

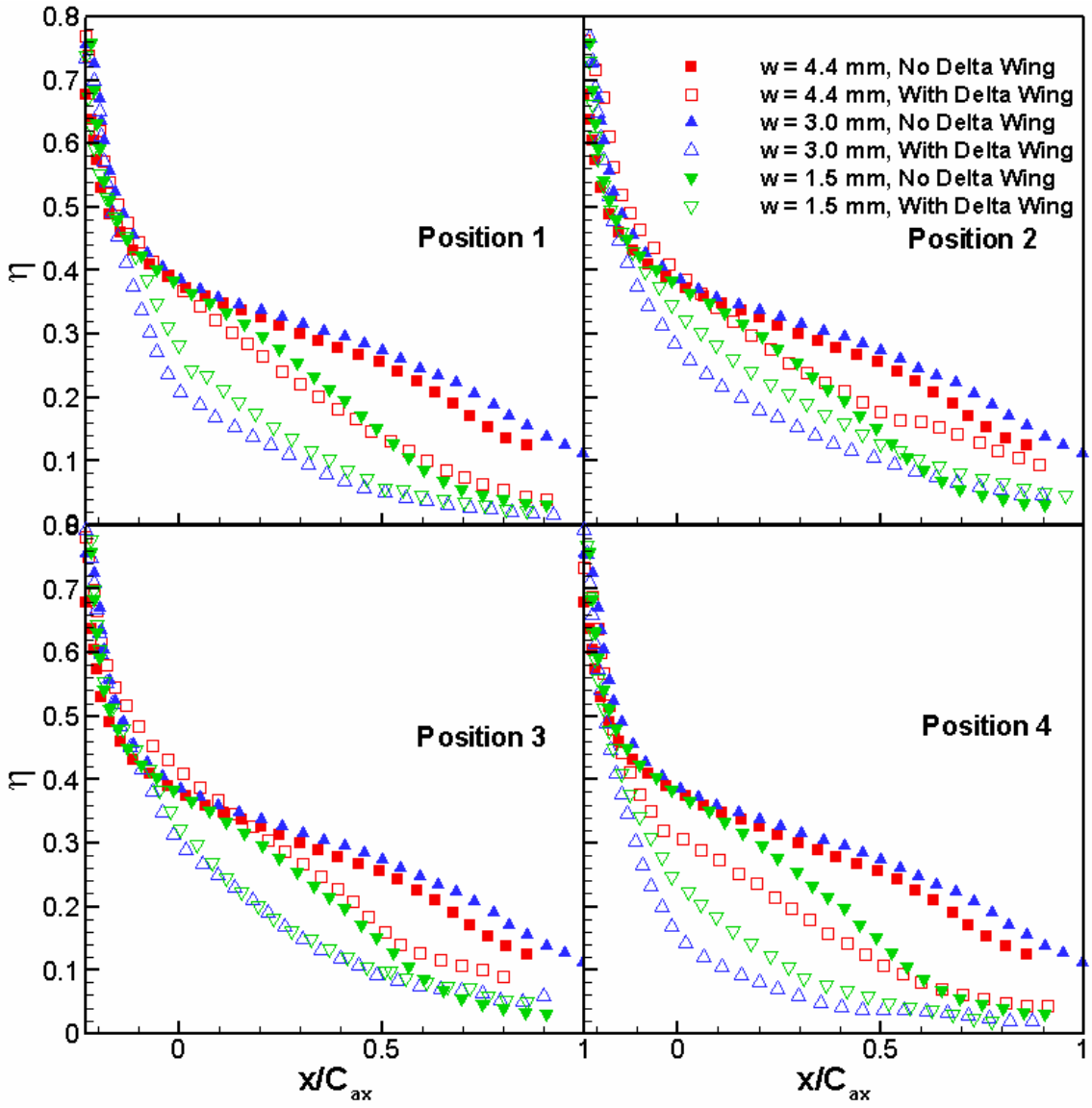

Figure 24: Comparison of Laterally Averaged Film Cooling Effectiveness on the Platform for Various Slot Widths, $\theta = 45°$ and $m_s = 1.5\%$

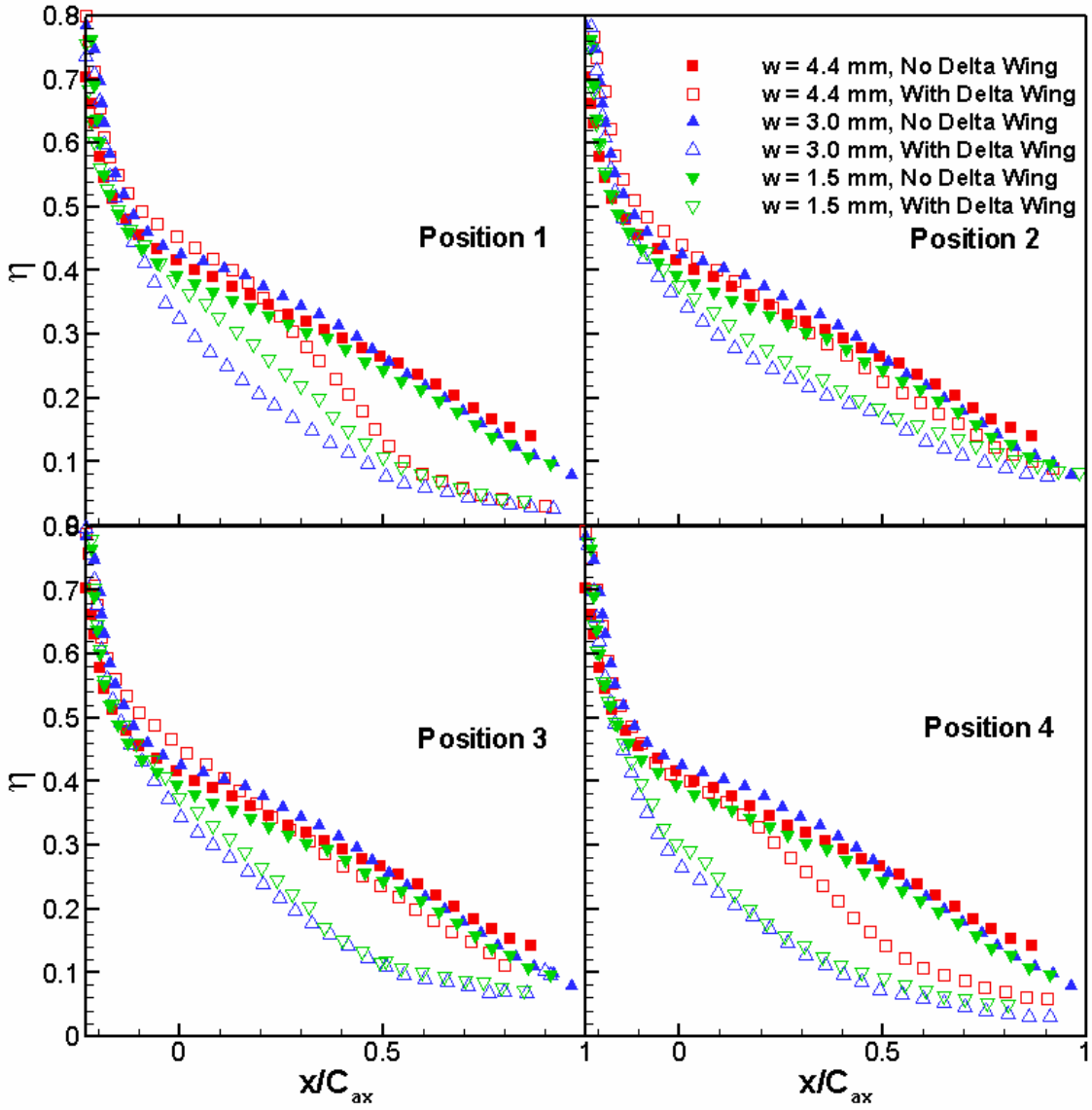

Figure 25: Comparison of Laterally Averaged Film Cooling Effectiveness on the Platform for Various Slot Widths, $\theta = 45°$ and $m_s = 2.0\%$

Figure 23 shows the same results for m_s = 1.0%. Without a delta wing, the 3.0 mm slot again gives the highest effectiveness. It appears that increasing the momentum of the coolant can increase the effectiveness to a point, but when the slot is too narrow, the coolant lifts off the endwall and mixes into the mainstream earlier. However, when the delta wing is added, the effect is strongest for the 3.0 mm slot, such that the effectiveness with the 3.0 mm slot is less than either of the other sizes.

In Figure 24, for a coolant flow rate of 1.5%, the two larger slot sizes give similar effectiveness without the delta wing, while the effectiveness for the 1.5 mm slot is much lower. For this flow rate, the momentum of the coolant passing through the 1.5 mm slot seems to be too high to stay near the surface. When the delta wing is added, the effectiveness of the 3.0 mm slot is reduced the most, and the effectiveness for the 4.4 mm slot is much higher than the two smaller sizes.

For a coolant flow rate of 2.0%, the effect of the slot width is minimized. Though the film cooling effectiveness distributions seen in Figures 8, 14, and 15 are different, the laterally averaged effectiveness is very similar. As previously noted, the smallest slot width causes the coolant to be pushed farther along the suction side of the passage, while the pressure side is left uncooled. This illustrates the importance of considering detailed effectiveness distributions, in addition to averaged values.

Figures 22 through 25 indicate that without the delta wing, the 3.0 mm slot gives the best results, followed by the 4.4 mm slot. This would indicate that the effectiveness increases with slot width until some optimum width is reached. It is unexpected that the 3.0 mm slot is the best of the three for all four blowing rates. Apparently of the three widths tested the 3.0 mm slot gives the best combination of coolant quantity and momentum.

When the delta wing is added, the 4.4 mm slot gives the best results, followed by the 1.5 mm slot. It is quite unexpected that the middle width would give the lowest effectiveness, especially since it gives the highest effectiveness without the delta wing.

The momentum of the coolant affects the film cooling effectiveness in two ways. It helps the coolant to continue along the platform, but it also affects the secondary flows in the passage. Without the delta wing, a higher momentum tends to move the coolant farther along the passage, but it also increases the secondary flows, reducing the effectiveness in key areas, such as the pressure side downstream of the passage vortex and under the horseshoe vortex.

With the delta wing, flow is complicated by an additional vortex. This vortex interacts with both the coolant flow and the secondary flows. Depending on the position of the delta wing, the delta wing vortex may tend to increase or decrease the secondary flows. However, with increasing coolant momentum, the coolant can disrupt the delta wing vortex, therefore decreasing its effect on the secondary flows. Due to this complicated flow, the dependence of film cooling effectiveness on slot width is also complex.

Figure 26 gives additional insight into the effect of slot width. The effectiveness across the line AB is plotted from the pressure side (A) to the suction side (B). With a blowing rate of 0.5%, the effectiveness in all cases is lower on the pressure side, due to the passage cross flow. As the blowing rate is increased, the effectiveness distribution for some cases becomes more uniform, especially for the larger slot widths without the delta wing. This shows the many effects that coolant momentum has on film cooling.

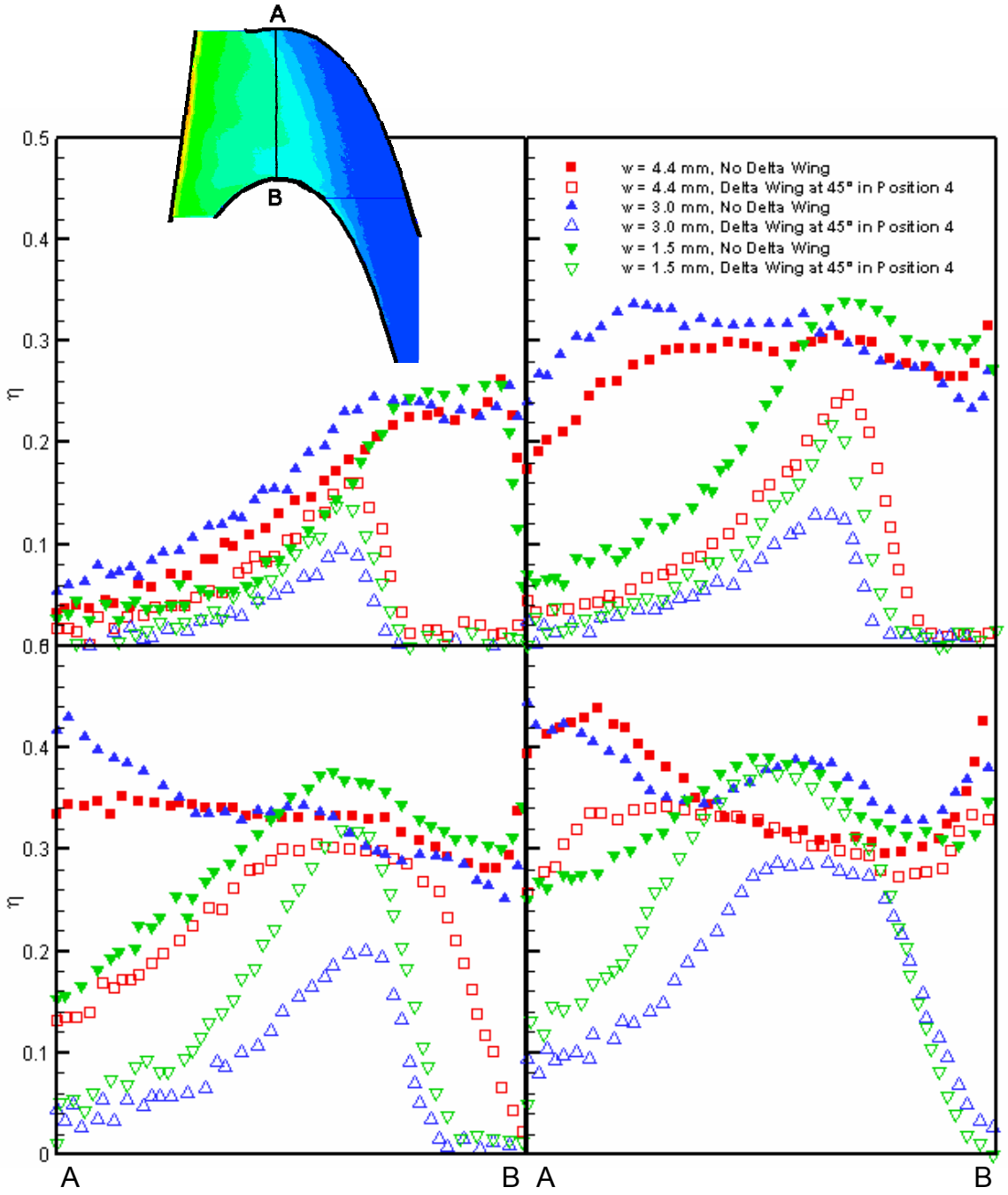

Figure 26: Comparison of Pitchwise Film Cooling Effectiveness for Various Slot Widths and Blowing Rates, Without Delta Wing and With Delta Wing in Position 4 ($\theta = 45°$)

Expected Heat Transfer Coefficients

Film cooling design requires knowledge of both the film cooling effectiveness and the convective heat transfer coefficient at each point on the surface. With these, one can determine the heat flux between the film layer and the surface. Though no heat transfer coefficients were measured in this study, one can make predictions about the heat transfer coefficient distributions based on previous studies and the current film cooling effectiveness distributions. In general, heat transfer coefficients will increase from the leading edge toward the trailing edge as the mainstream velocity increases. Due to the formation of the horseshoe vortex, high heat transfer coefficients will be present near the leading edge. Also, under the passage vortex and other vortices, the heat transfer coefficients will be higher than in adjacent areas. Film cooling injection has been shown to increase the heat transfer coefficients near the slot. However, in cases where the coolant disrupts the secondary flows, the heat transfer coefficients will not be as high in the location of those secondary flows. The vortex created by the delta wing would also increase the heat transfer coefficients.

In general, the areas near the slot have high film cooling effectiveness but would also have high heat transfer coefficients and would not be overcooled. Areas under secondary flows in the passage or from the delta wing would have low film cooling effectiveness and high heat transfer coefficients and may be undercooled. The area near the pressure side of the blade tends to have low film cooling effectiveness due to the passage cross flow, but it would also have lower heat transfer coefficients than on the suction side.

CONCLUSIONS

The film cooling effectiveness distribution on the platform of a linear cascade of turbine blades was measured experimentally for coolant injected through a simulated stator-rotor seal upstream of the blades. Rods and delta wings were placed upstream to simulate the effect of the upstream vane. The seal width was also varied.

The unsteady wake formed at the trailing edge of a vane was found to have little impact on cooling of the downstream rotor platform. The passage vortex created in the vane may significantly alter the downstream rotor platform cooling, depending on the strength of the vortex in a particular vane. In general, the passage vortex created in the vane reduces the film cooling effectiveness on the rotor platform. Due to the momentum of the coolant, the effect of the passage vortex is small near the slot. The distance from the slot which is relatively unaffected by the upstream passage vortex depends on the coolant flow rate and momentum. For higher flow rates, a larger portion of the passage is unaffected by the upstream vane secondary flows.

As the width of the stator-rotor seal is reduced, the momentum of the coolant is increased for the same mass flow rate. This yields higher film cooling effectiveness close to the slot, as the mainstream flow is unable to penetrate the coolant flow. Farther downstream, the effect of the secondary flows is stronger, such that the film cooling effectiveness on the suction side is higher, but it is lower on the pressure side. The effect of the upstream passage vortex is also stronger for narrower seals.

Past studies have indicated that flow from the stator-rotor seal can effectively cool a large portion of the rotor platform. However, care should be taken in cooling designs to consider the strength of the passage vortex, as well as the possible misalignment of the stator and rotor, since these factors can significantly reduce the film cooling effectiveness.

Recommendations

In order to give a complete picture of effects of seal width and the upstream vane on platform film cooling, heat transfer coefficients on the platform should be measured. The effect of other forms of misalignment, such as forward- or backward-facing steps could also be studied in combination with the varied seal width and delta wings. In order to fully understand the effect of varying slot width, particularly with the delta wing, it would be beneficial to test a wider range of widths.

REFERENCES

[1] Han, J.C., Dutta, S., and Ekkad, S.V., 2000, Gas *Turbine Heat Transfer and Cooling Technology*, Taylor and Francis, New York.

[2] Langston, L.S., "Secondary Flows in Axial Turbines – A Review," Annals of the New York Academy of Sciences, **934**, pp. 11-26.

[3] Chyu, M.K., 2001, "Heat Transfer near Turbine Nozzle Endwall," Annals of the New York Academy of Sciences, **934**, pp. 27-36.

[4] Simon, T.W. and Piggush, J.D., 2006, "Turbine Endwall Aerodynamics and Heat Transfer," AIAA J. of Propulsion and Power, **22**, pp. 310-312.

[5] Langston, L.S., Nice, L.M., and Hooper, R.M., 1977, "Three-Dimensional Flow within a Turbine Cascade Passage," ASME J. Turbomachinery, **99**, pp. 21-28.

[6] Langston, L.S., 1980, "Crossflows in a Turbine Cascade Passage," ASME J. Engineering for Power, **102**, pp. 866-874.

[7] Goldstein, R.J. and Spores, R.A., 1988, "Turbulent Transport on the Endwall in the Region between Adjacent Turbine Blades." ASME J. Heat Transfer, **110**, pp. 862-869.

[8] Wang, H.P., Olson, S.J., and Goldstein, R.J., 1997, "Flow Visualization in a Linear Turbine Cascade of High Performance Turbine Blades," ASME J. Turbomachinery, **119**, pp. 1-8.

[9] Takeishi, K., Matsuura, M., Aoki, S., and Sato, T., 1990, "An Experimental Study of Heat Transfer and Film Cooling on Low Aspect Ratio Turbine Nozzles," ASME J. Turbomachinery, **112**, pp. 488-496.

[10] Harasgama, S.P. and Burton, C.S., 1992, "Film Cooling Research on the Endwall of a Turbine Nozzle Guide Vane in a Short Duration Annular Cascade: Part 1 – Experimental Technique and Results," ASME J. Turbomachinery, **114**, pp. 734-740.

[11] Jabbari, M.Y., Marston, K.C., Eckert, E.R.G., and Goldstein, R.J., 1996, "Film Cooling of the Gas Turbine Endwall by Discrete-Hole Injection," ASME J. Turbomachinery, **118**, pp. 278-284.

[12] Friedrichs, S., Hodson, H.P., and Dawes, W.N., 1996, "Distribution of Film-Cooling Effectiveness on a Turbine Endwall Measured Using the Ammonia and Diazo Technique," ASME J. Turbomachinery, **118**, pp. 613-621.

[13] Friedrichs, S., Hodson, H.P., and Dawes, W.N., 1997, "Aerodynamic Aspects of Endwall Film Cooling," ASME J. Turbomachinery, **119**, pp. 786-793.

[14] Friedrichs, S., Hodson, H.P., and Dawes, W.N., 1999, "The Design of an Improved Endwall Film Cooling Configuration," ASME J. Turbomachinery, **121**, pp. 772-780.

[15] Barigozzi, G., Benzoni, G., Franchini, G., and Derdichizzi, A., 2005, "Fan-Shaped Hole Effects on the Aero-Thermal Performance of a Film Cooled Endwall," ASME paper no. GT2005-68544.

[16] Blair, M.F., 1974, "An Experimental Study of Heat Transfer and Film Cooling on Large-Scale Turbine Endwall," ASME J. Heat Transfer, **96**, pp. 524-529.

[17] Granser, D. and Schulenberg, T., 1990, "Prediction and Measurement of Film Cooling Effectiveness for a First-Stage Turbine Vane Shroud," ASME paper no. 90-GT-95.

[18] Roy, R.P., Squires, K.D., Gerendas, M., Song, S., Howe, W.J., and Ansari, A., 2000, "Flow and Heat Transfer at the Hub Endwall of Inlet Vane Passages – Experiments and Simulations," ASME paper no. 2000-GT-198.

[19] Burd, S.W., Satterness, C.J., and Simon, T.J., 2000, "Effects of Slot Bleed Injection over a Contoured End Wall on Nozzle Guide Vane Cooling Performance: Part II – Thermal Measurements," ASME paper no. 2000-GT-200.

[20] Oke, R., Simon, T., Shih, T., Zhu, B., Lin, Y.L., and Chyu, M., 2001, "Measurements over a Film-Cooled Contoured Endwall with Various Coolant Injection Rates," ASME paper no. 2001-GT-0140.

[21] Oke, R.A. and Simon, T.W., 2002, "Film Cooling Experiments with Flow Introduced Upstream of a First Stage Nozzle Guide Vane through Slots of Various Geometries," ASME paper no. GT-2002-30169.

[22] Nicklas, M., 2001, "Film-Cooled Turbine Endwall in a Transonic Flow Filed: Part II – Heat Transfer and Film Cooling Effectiveness," ASME J. Turbomachinery, **123**, pp. 720-729.

[23] Liu, G., Liu, S., Zhu, H., Lapworth, B.C., and Forest, A.E., 2004, "Endwall Heat Transfer and Film Cooling Measurements in a Turbine Cascade with Injection Upstream of Leading Edge," Heat Transfer – Asian Research, **33**, pp. 141-152.

[24] Zhang, L.J. and Jaiswal, R.S., 2001, "Turbine Nozzle Endwall Film Cooling Study Using Pressure-Sensitive Paint," ASME J. Turbomachinery, **123**, pp. 730-735.

[25] Zhang, L.J. and Moon, H.K., 2003, "Turbine Nozzle Endwall Inlet Film Cooling – The Effect of a Backward Facing Step," ASME paper no. GT2003-38319.

[26] Knost, D.G. and Thole, K.A., 2004, "Adiabatic Effectiveness Measurements of Endwall Film Cooling for a First Stage Vane," ASME paper no. GT2004-53326.

[27] Cardwell, N.D., Sundaram, N., and Thole, K.A., 2005, "Effects of Mid-Passage Gap, Endwall Misalignment and Roughness on Endwall Film-Cooling," ASME paper no. GT2005-68900.

[28] Wright, L.M., Gao, Z., Yang, H., and Han, J.C., 2006, "Film Cooling Effectiveness Distribution on a Gas Turbine Blade Platform with Inclined Slot Leakage and Discrete Film Hole Flows," ASME paper no. GT2006-90375.

[29] Wright, L.M., Blake, S., and Han, J.C., 2006, "Effectiveness Distributions on Turbine Blade Cascade Platforms through Simulated Stator-Rotor Seals," AIAA paper no. AIAA-2006-3402.

[30] Wright, L.M., Blake, S., and Han, J.C., 2006, "Film Cooling Effectiveness Distributions on a Turbine Blade Cascade Platform with Stator-Rotor Purge and Discrete Film Holes Flows," ASME paper no. IMECE2006-15092.

[31] Han, J.-C., Zhang, L., and Ou, S., 1993, "Influence of Unsteady Wake on Heat Transfer Coefficient from a Gas Turbine Blade," ASME J. Heat Transfer, **115**, pp. 904-911.

[32] Ou, S., Han, J.-C., Mehendale, A.B., and Lee, C.P., 1994, "Unsteady Wake Over a Linear Turbine Blade Cascade with Air and CO2 Film Injection: Part I---Effect on Heat Transfer Coefficients," ASME J. Turbomachinery, **116**, pp. 721-729.

[33] Zhang, L., and Han, J.-C., "Influence of Mainstream Turbulence on Heat Transfer Coefficients from a Gas Turbine Blade," ASME J. Heat Transfer, 116, pp. 896-903.

[34] Zhang, L., and Han, J.-C., "Combined Effect of Free-Stream Turbulence and Unsteady Wake on Heat Transfer Coefficients from a Gas Turbine Blade," ASME J. Heat Transfer, **117**, pp. 296-302.

[35] Mhetras, S., and Han, J.C., 2006, "Effect of Unsteady Wake on Full Coverage Film-Cooling Effectiveness for a Gas Turbine Blade," AIAA paper no. 2006-3403.

[36] Sauer, H., Muller, R., and Vogerler, K., 2000, "Reduction of Secondary Flow Losses in Turbine Cascades by Leading Edge Modification at the Endwall," ASME paper no. 2000-GT-0473.

[37] Zess, G.A. and Thole, K.A., 2002, "Computational Design and Experimental Evaluation of Using a Leading Edge Fillet on a Gas Turbine Vane," ASME Journal of Turbomachinery, **124**, pp. 167 – 175.

[38] Becz, S., Majewski, M.S., and Langston, L.S., 2003, "Leading Edge Modification Effects on Turbine Cascade Endwall Loss," ASME paper no. GT2003-38898.

[39] Shih, T.I-P. and Lin, Y.-L., 2002, "Controlling Secondary – Flow Structure by Leading – Edge Airfoil Fillet and Inlet Swirl to Reduce Aerodynamic Loss and Surface Heat Transfer," ASME paper no. GT-2002-30529.

[40] Lethander, A.T., Thole, K.A., Zess, G., and Wagner, J., 2004, "Vane – Endwall Junction Optimization to Reduce Turbine Vane Passage Adiabatic Wall Temperatures," AIAA Journal of Propulsion and Power, **20**, pp. 1105-1116.

[41] Zhang, L. and Han, J.C., 1994, "Influence of Mainstream Turbulence on Heat Transfer Coefficients from a Gas Turbine Blade," ASME J. Heat Transfer, **116**, pp. 896-903.

[42] Hermanson, K., Kern, S., Picker, G., and Parneix, S., 2003, "Predictions of External Heat Transfer for Turbine Vanes and Blades with Secondary Flow Fields," ASME J. Turbomachinery, **125**, pp. 107-113.

[43] Wright, L.M., Gao, Z., Varvel, T.A., and Han, J.C., 2005, "Assessment of Steady State PSP, TSP, and IR Measurement Techniques for Flat Plate Film Cooling," ASME paper no. HT2005-72363.

[44] Gao, Z., Wright, L.M., and Han, J.C., 2005, "Assessment of Steady State PSP and Transient IR Measurement Techniques for Leading Edge Film Cooling," ASME paper no. IMECE2005-80146.

APPENDIX A

DETAILED FILM COOLING EFFECTIVENESS DISTRIBUTIONS COMPARING VARIOUS UPSTREAM CONDITIONS FOR ALL FLOW RATES

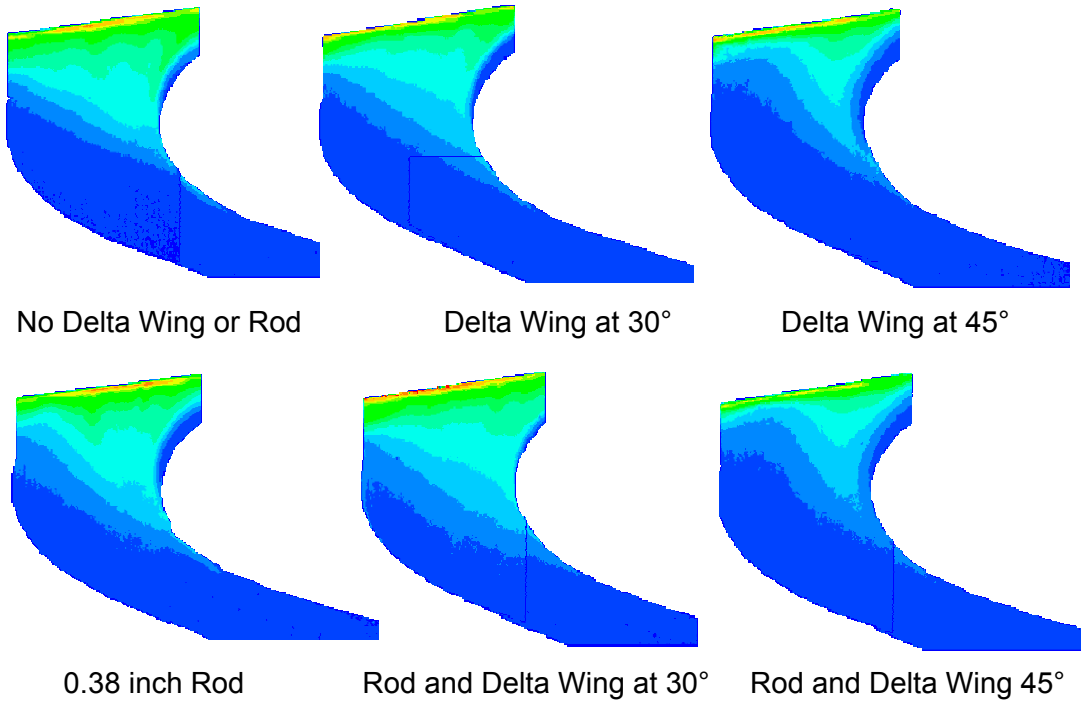

Figure A-1: w = 4.4 mm, m_s = 0.5%, Position 1

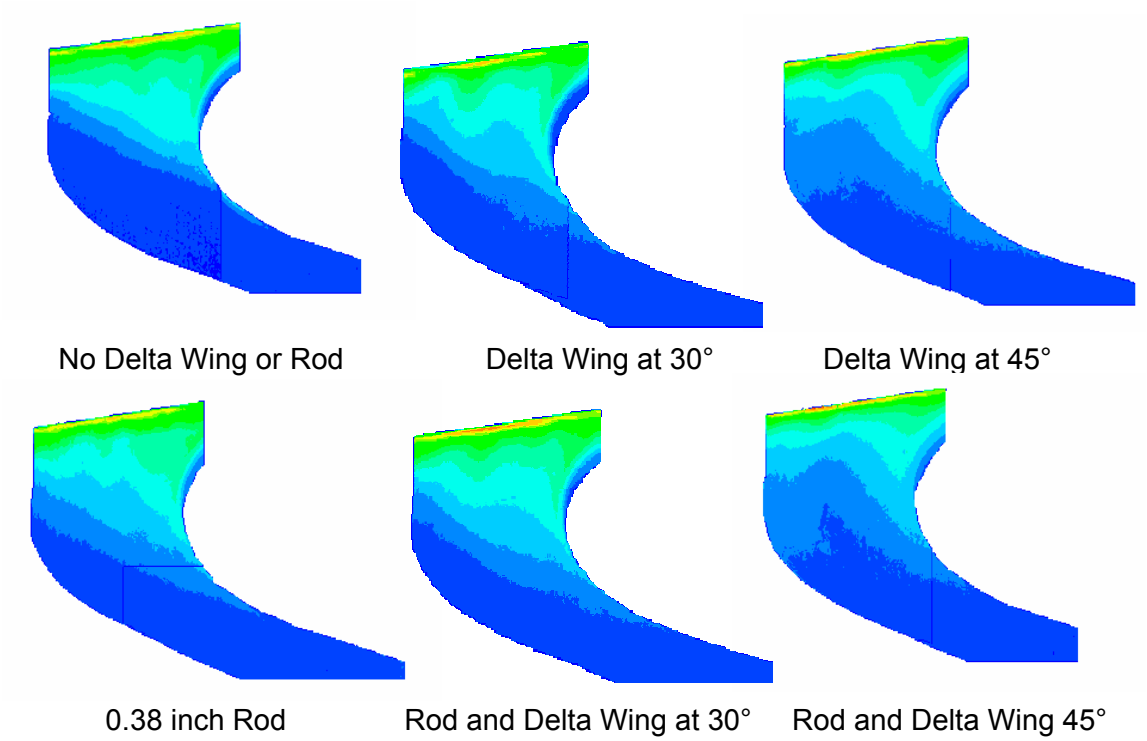

Figure A-2: w = 4.4 mm, ms = 0.5%, Position 2

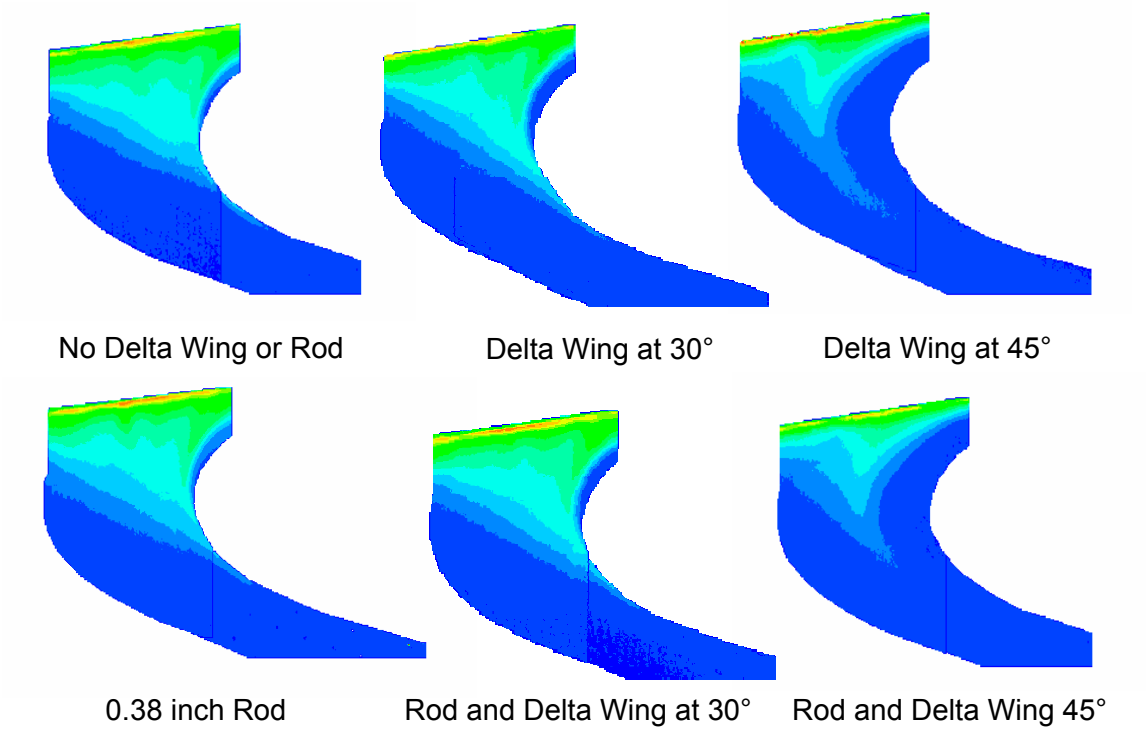

Figure A-3: w = 4.4 mm, ms = 0.5%, Position 3

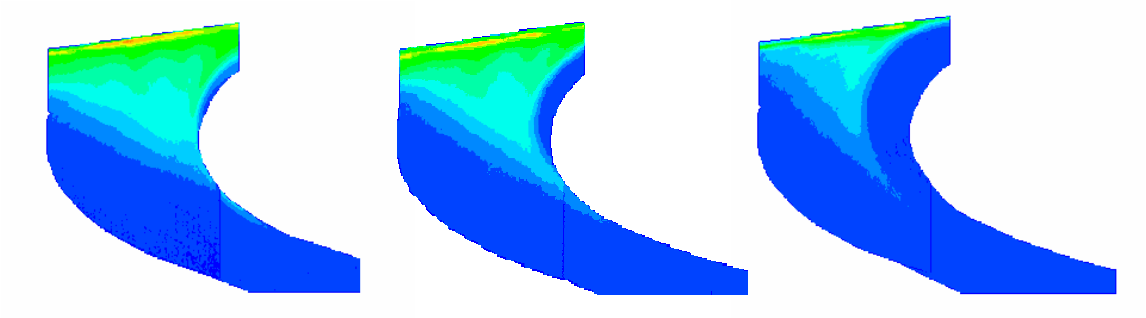

No Delta Wing or Rod Delta Wing at 30° Delta Wing at 45°

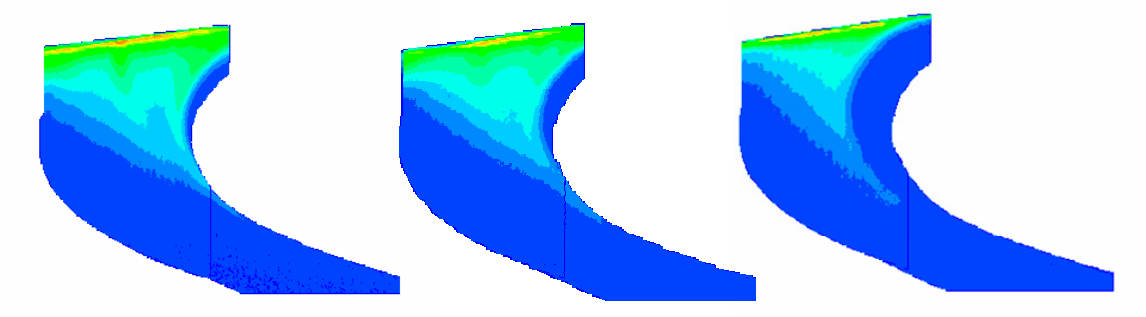

0.38 inch Rod Rod and Delta Wing at 30° Rod and Delta Wing 45°

Figure A-4: w = 4.4 mm, ms = 0.5%, Position 4

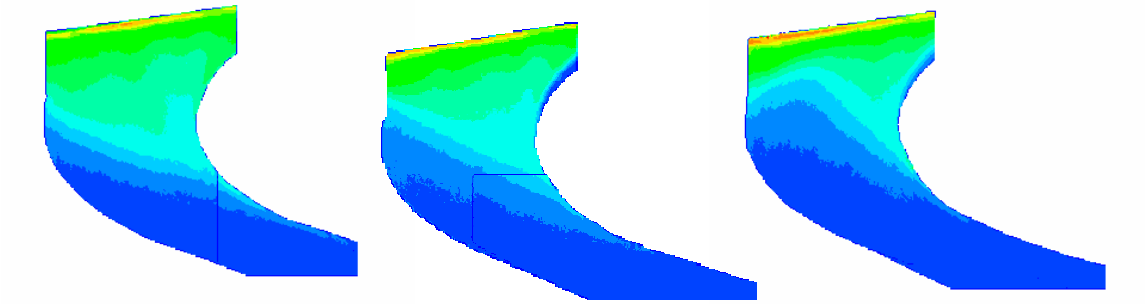

No Delta Wing or Rod Delta Wing at 30° Delta Wing at 45°

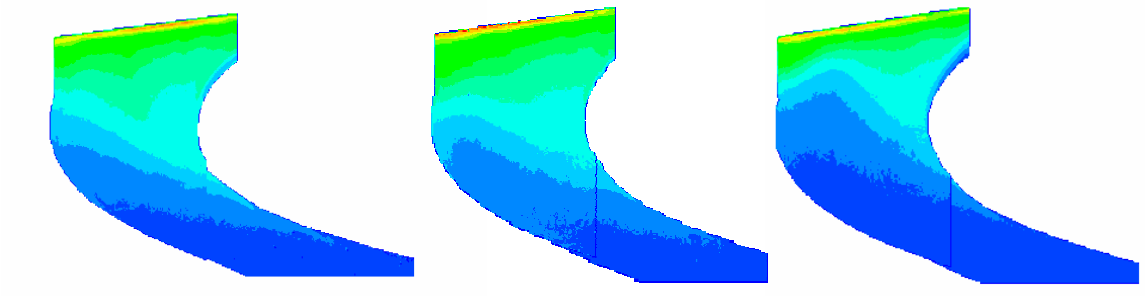

0.38 inch Rod Rod and Delta Wing at 30° Rod and Delta Wing 45°

Figure A-5: w = 4.4 mm, ms = 1.0%, Position 1

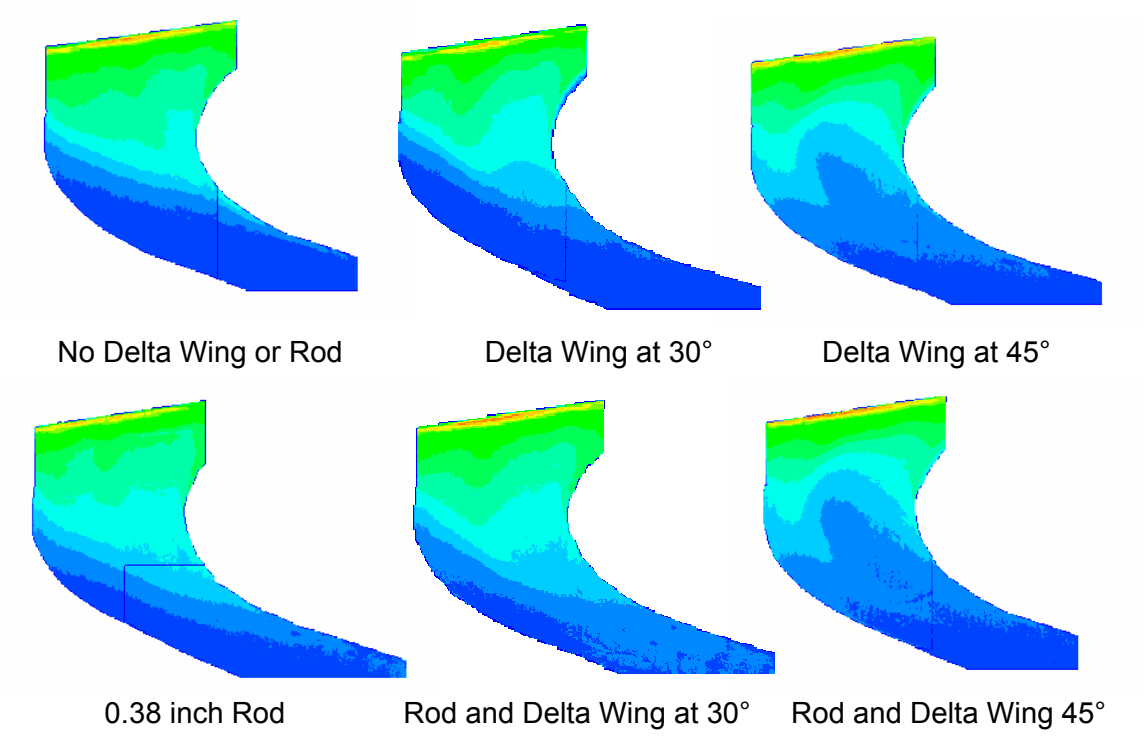

Figure A-6: w = 4.4 mm, ms = 1.0%, Position 2

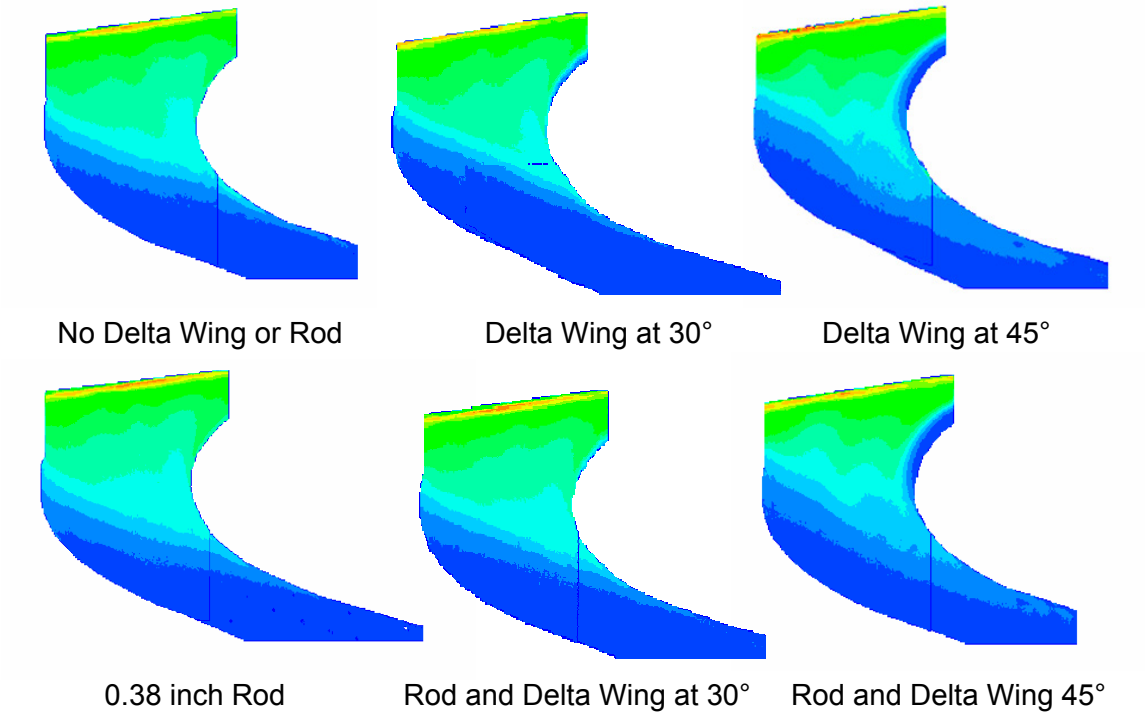

Figure A-7: w = 4.4 mm, ms = 1.0%, Position 3

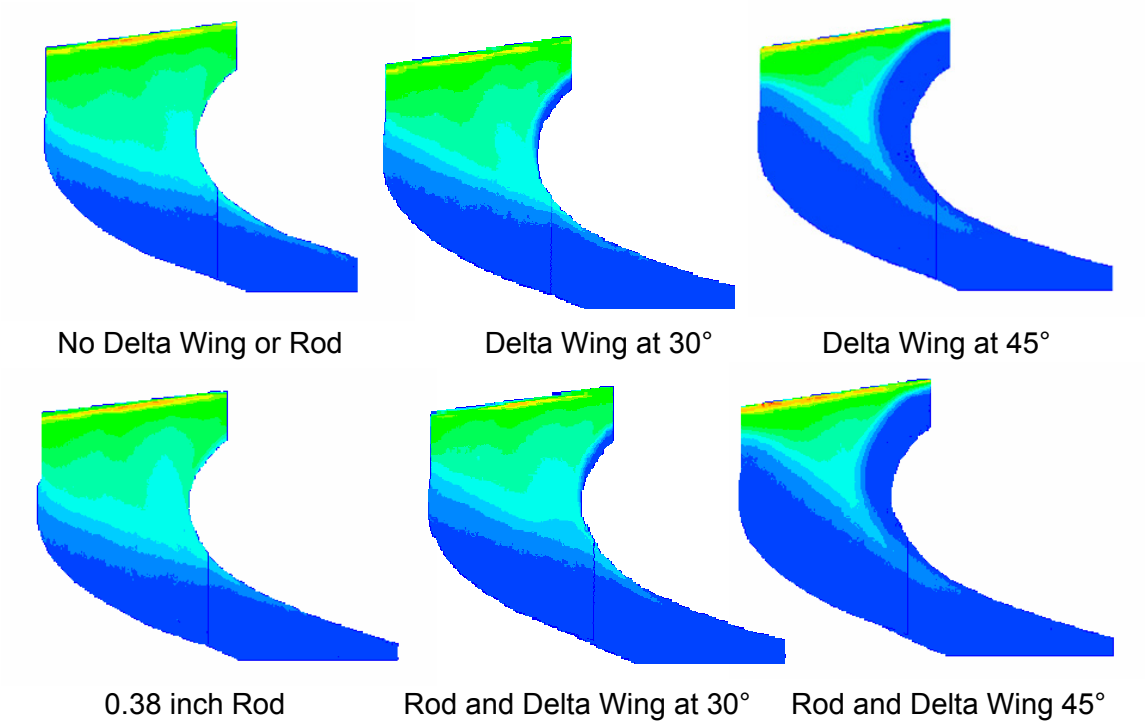

Figure A-8: w = 4.4 mm, ms = 1.0%, Position 4

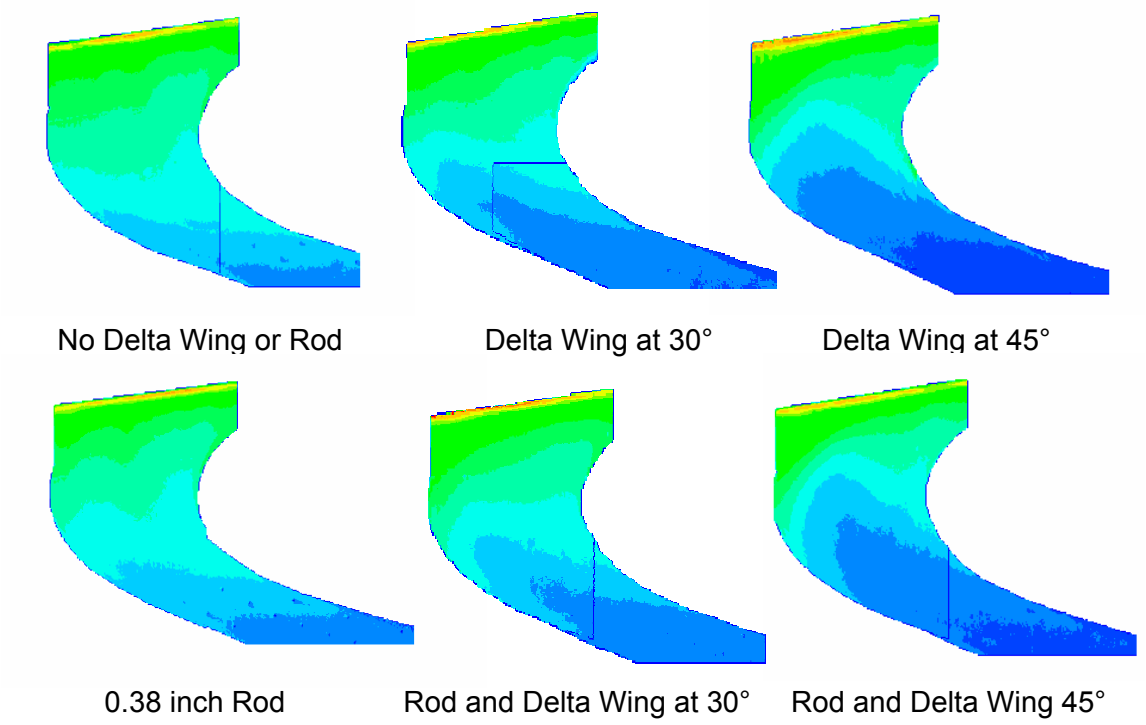

Figure A-9: w = 4.4 mm, ms = 1.5%, Position 1

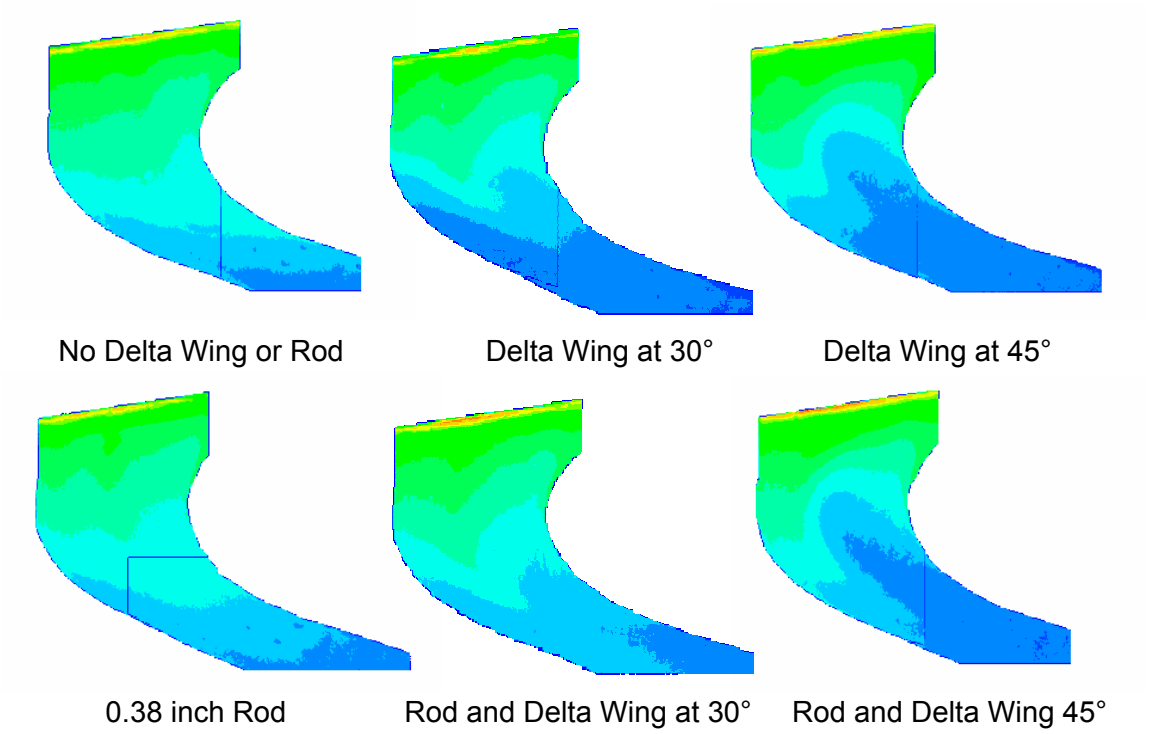

Figure A-10: w = 4.4 mm, ms = 1.5%, Position 2

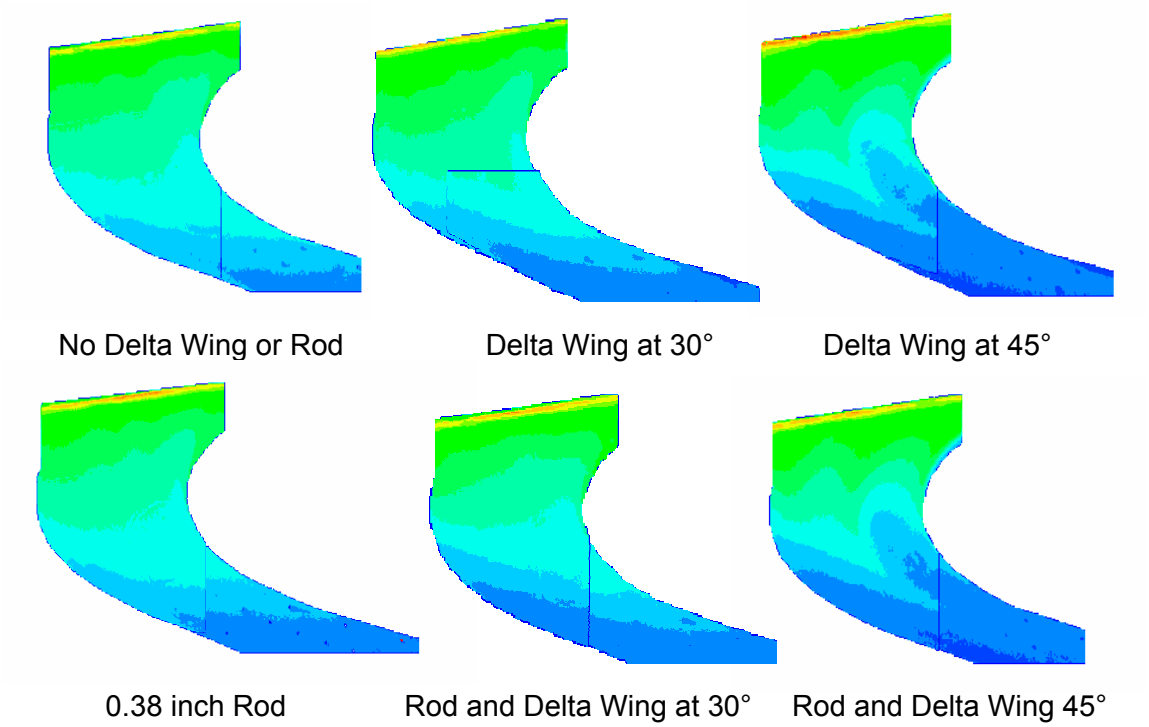

Figure A-11: w = 4.4 mm, ms = 1.5%, Position 3

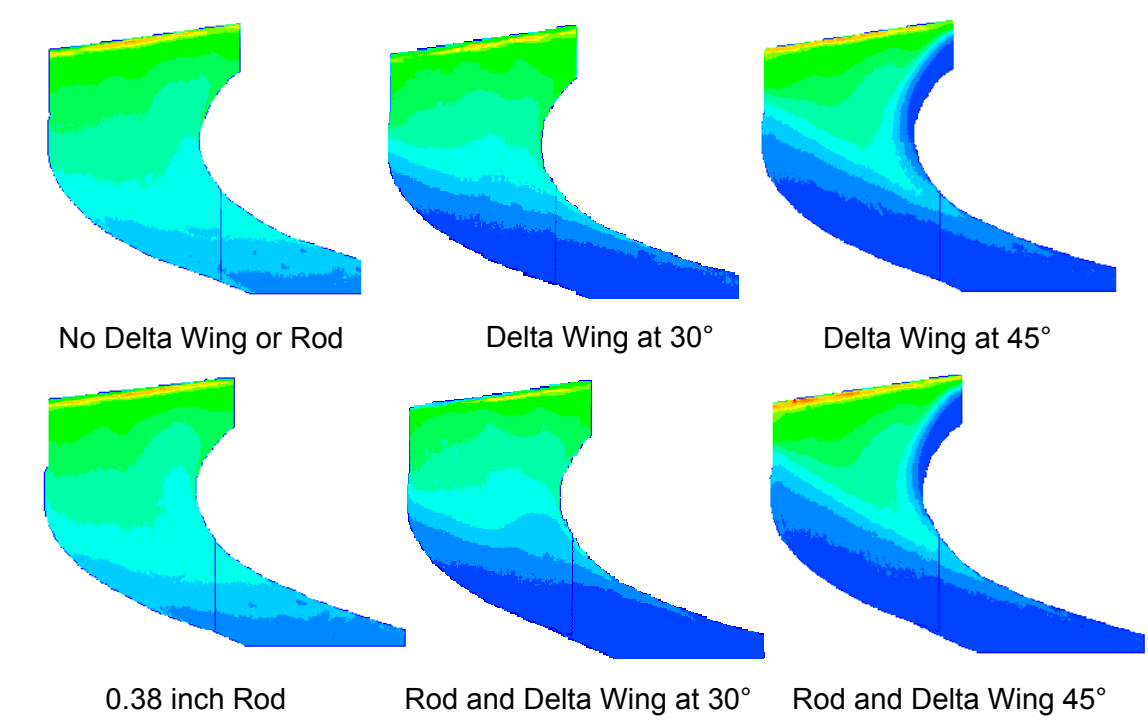

Figure A-12: w = 4.4 mm, ms = 1.5%, Position 4

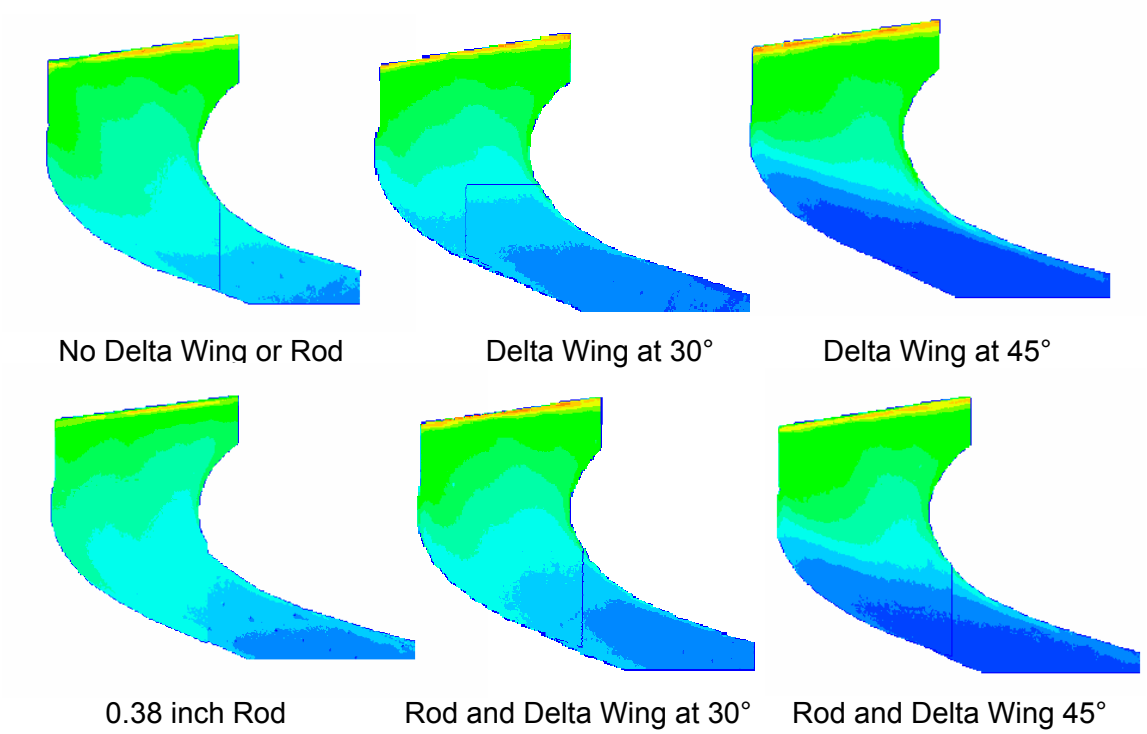

Figure A-13: w = 4.4 mm, ms = 2.0%, Position 1

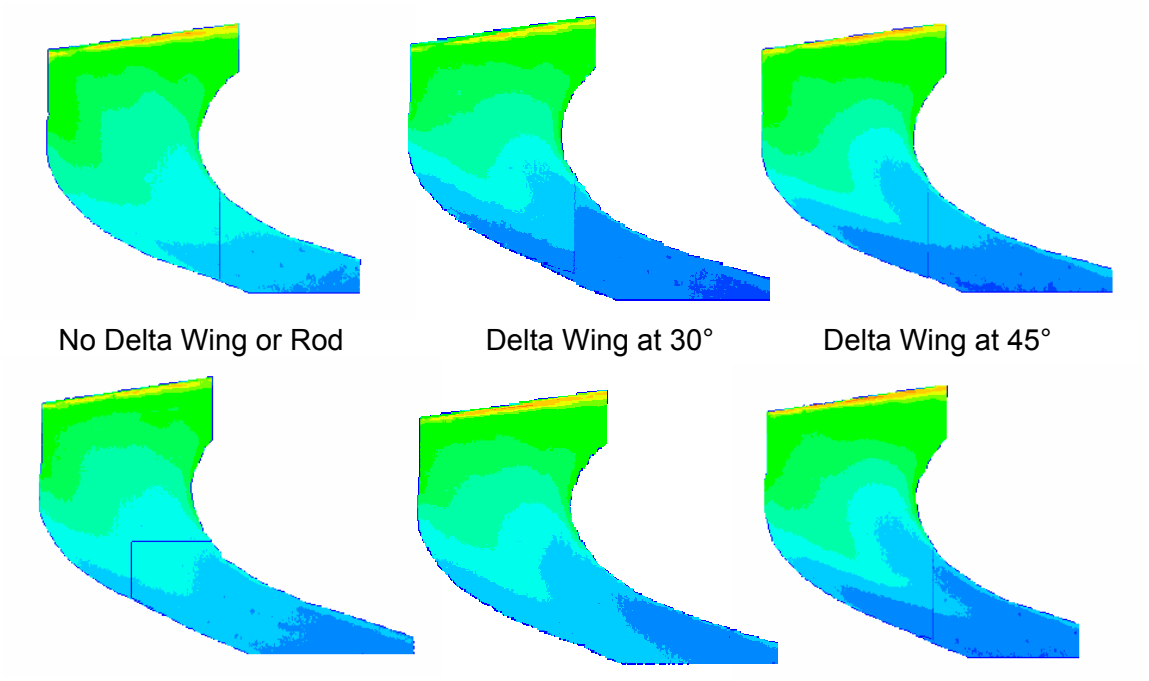

Figure A-14: w = 4.4 mm, ms = 2.0%, Position 2

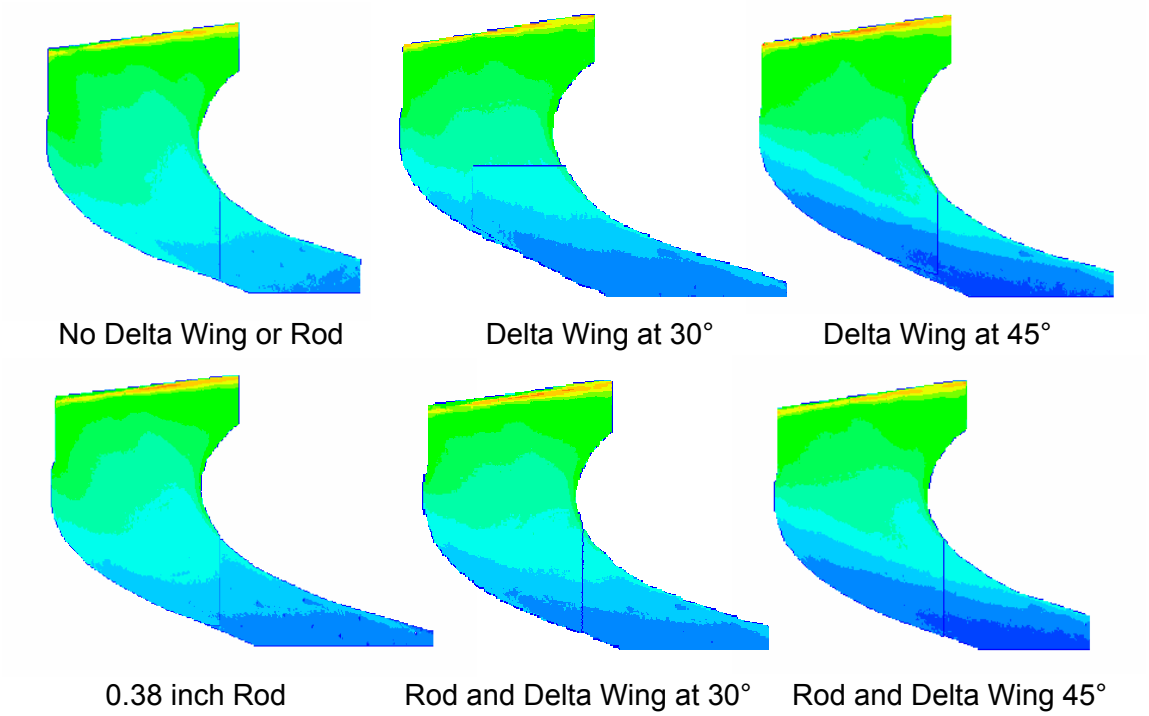

Figure A-15: w = 4.4 mm, ms = 2.0%, Position 3

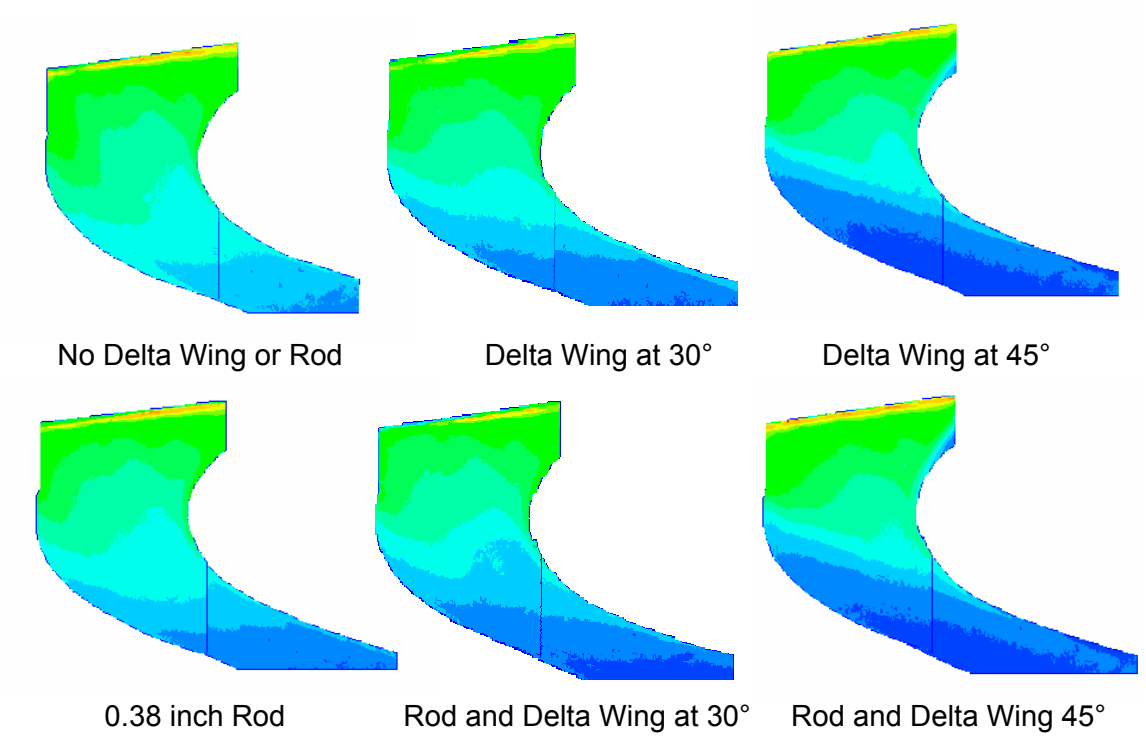

Figure A-16: w = 4.4 mm, ms = 2.0%, Position 4

APPENDIX B

DETAILED FILM COOLING EFFECTIVENESS DISTRIBUTIONS COMPARING VARIOUS SLOT WIDTHS FOR VARIOUS UPSTREAM CONDITIONS

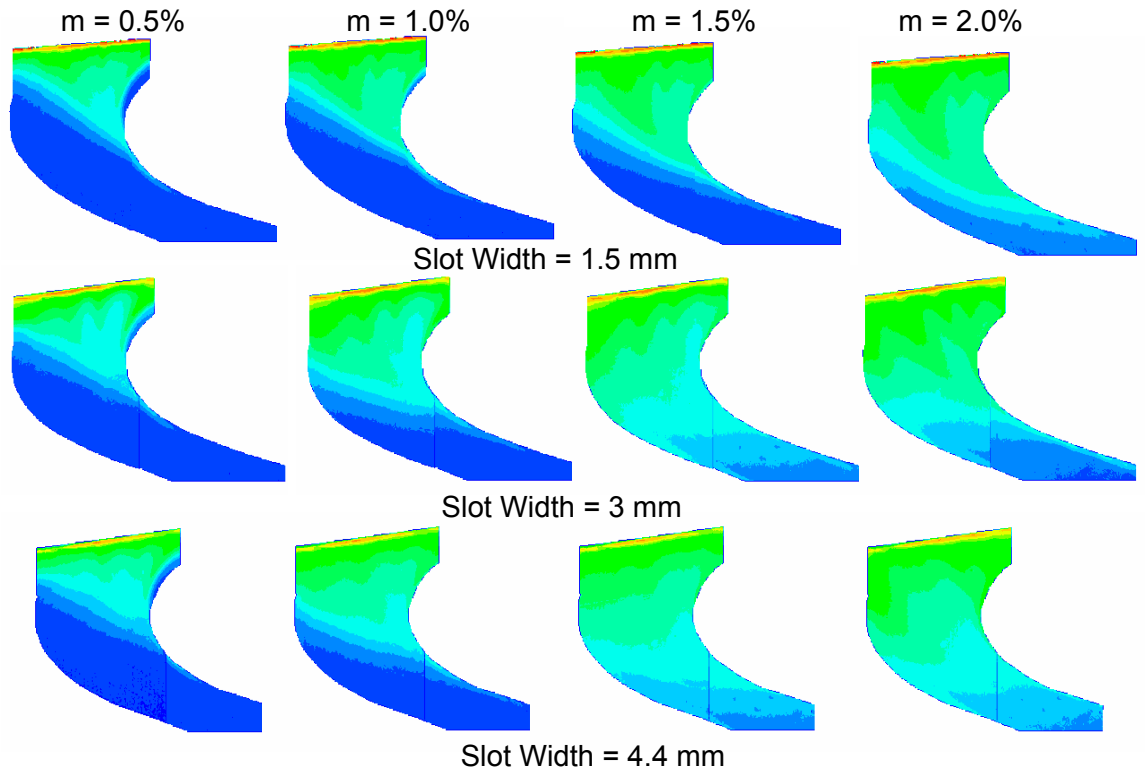

Figure A-17: Tu = 5%, No Rod or Delta Wing

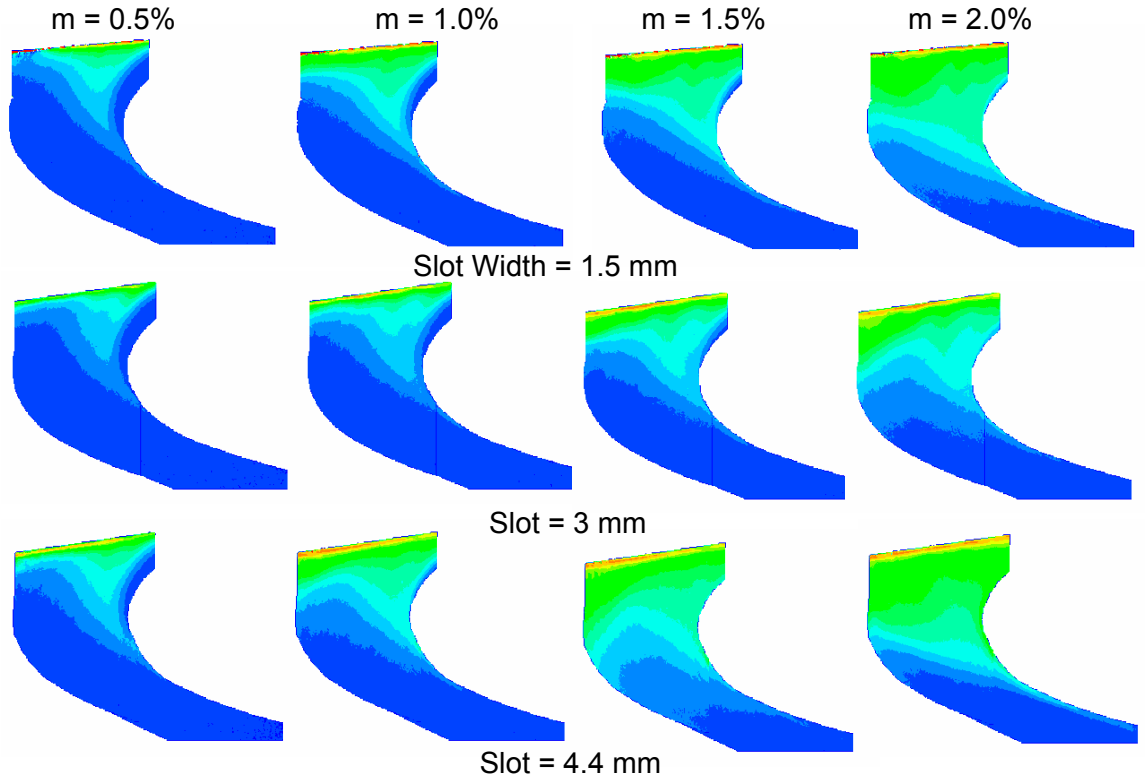

Figure A-18: Delta Wing at 45°, Position 1

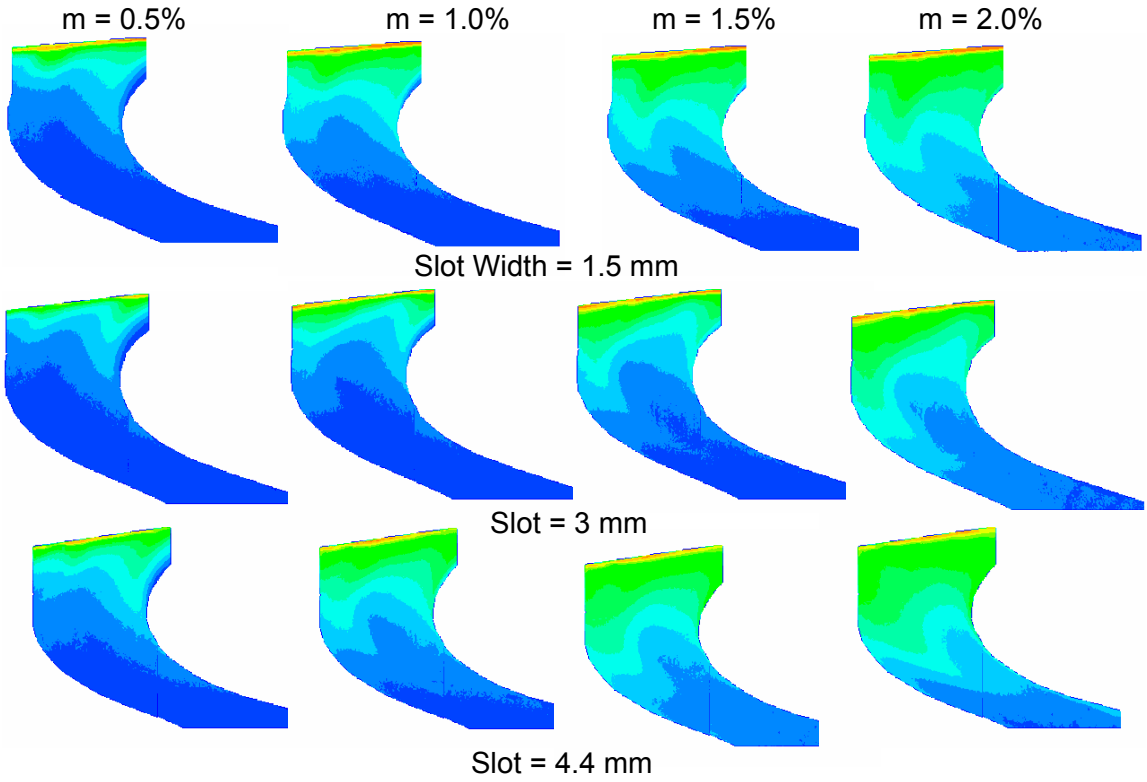

Figure A-19: Delta Wing at 45°, Position 2

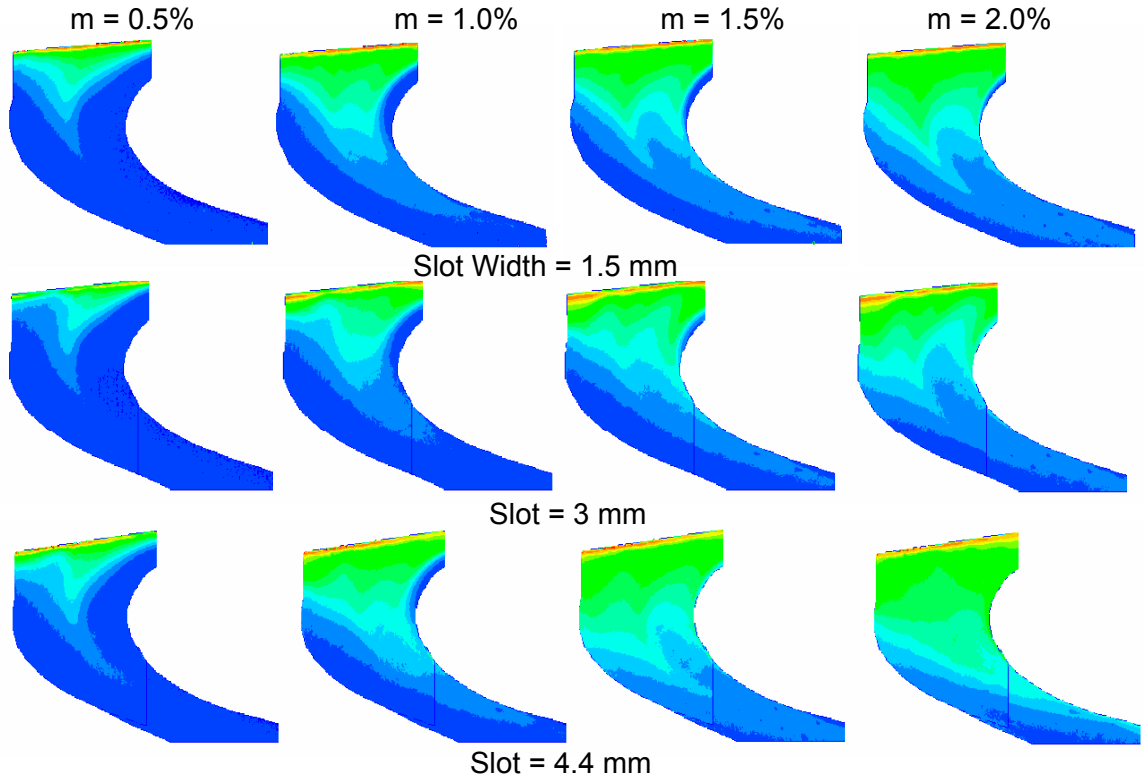

Figure A-20: Delta Wing at 45°, Position 3

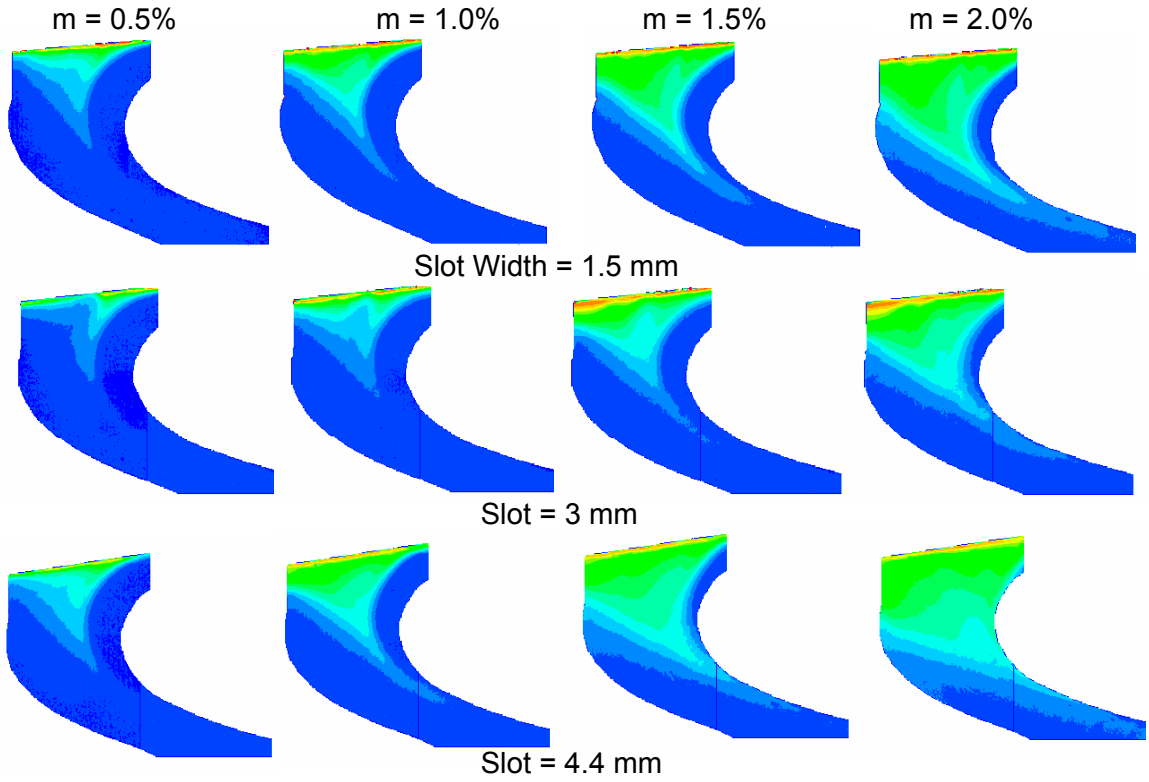

Figure A-21: Delta Wing at 45°, Position 4

VITA

Name: Sarah Anne Blake

Mailing Address: Turbine Heat Transfer Laboratory
Texas A&M University
3123 TAMU
College Station, TX 77843

Email Address: sarah_blake@tamu.edu

Hometown: Bucksport, Maine

Education: Bachelor of Science, 2004
Mechanical Engineering
University of Maine
Orono, Maine

Master of Science, 2007
Mechanical Engineering
Texas A&M University
College Station, Texas